CHARACTERIZATION OF PUTATIVE ACETATE KINASE IN THE PATHOGENIC YEAST, *CRYPTOCOCCUS NEOFORMANS*

A thesis presented to the faculty of the Graduate School of
Western Carolina University in partial fulfillment of the
requirements for the degree of Master of Science in Biology

By

Beth Ann Budden

Director: Dr. Indrani Bose
Assistant Professor of Biology
Biology Department

Committee Members: Dr. Seán O'Connell, Biology
Dr. Sabine Rundle, Biology

April 2013

ACKNOWLEDGEMENTS

First and foremost, I would like to thank my husband, Mark, and my daughters, Emma and Aspen, for their endless support and patience. Without it, this accomplishment would not have been possible. I'd also like to thank my mom, Cindy, and my sister, Steff, who kept my spirits up from afar.

I would like to thank my research advisor, Dr. Indi Bose, and my committee members, Drs. Sabine Rundle and Seán O'Connell, for their guidance as well as Dr. Greg Adkison, for serving as the reader for this thesis. I would also like to thank the WCU Biology faculty and staff who have generously offered assistance and equipment.

Last, but certainly not least, I would like to thank my undergraduate research advisor, Dr. Scott Mateer, for giving me the opportunity to engage in undergraduate research. Working in Dr. Mateer's lab was highly influential in my decision to pursue this Master's degree.

TABLE OF CONTENTS

LIST OF FIGURES

LIST OF TERMS/ABBREVIATIONS

gDNA.....genomic DNA
cDNA.....complementary DNA
mRNA.....messenger RNA
ack1Δ.....*ACK1* deletion strain
ACK1.....acetate kinase gene
ACT1.....actin gene
Ack1p.....acetate kinase protein
ackA.....acetate kinase gene (bacteria)
XFP.....xylulose 5-phosphate/fructose 6-phosphate phosphoketolase
PCR.....polymerase chain reaction
WT.....wild type (KN99 mat α)
KN99 mat α.....wild type (WT) strain
KN99 mat a.....opposite mating type of WT strain
YPD.....yeast, peptone, and dextrose medium
YNB.....yeast nitrogen base
SDS.....sodium dodecyl sulfate
RT.....room temperature
bp.....base pairs
Kb.....kilobases (x 1000 bp)

ABSTRACT

CHARACTERIZATION OF PUTATIVE ACETATE KINASE IN THE PATHOGENIC YEAST, *CRYPTOCOCCUS NEOFORMANS*

Beth Budden, M.S.

Western Carolina University (April 2013)

Director: Dr. Indrani Bose

The spherical, encapsulated basidiomycetous yeast, *Cryptococcus neoformans*, is an environmental opportunistic pathogen that has become a leading cause of mortality secondary to HIV/AIDS, particularly in sub-Saharan Africa (Park et al. 2009). Few chemotherapeutic agents are currently available to treat cryptococcosis, and growing concerns over resistance to some of these medications have emphasized the need for alternative treatments. By obtaining a thorough understanding of the metabolic pathways involved in the survival and pathogenicity of this organism it is hoped that pathways and/or proteins unique to the organism can be used as potential targets for chemotherapeutic agents (Casadevall and Perfect 1998). A homolog of an enzyme previously thought to exist only in bacteria, acetate kinase (AK), has been identified in certain lower eukaryotes including *C. neoformans*. To date, an acetate kinase homolog has not been found in higher eukaryotic organisms.

To get a better understanding of the role acetate kinase plays in *C. neoformans*, pre-constructed *ACK1* deletion strains (*ack1Δ*) were confirmed via cDNA analysis and Southern blot and were used in a variety of phenotype characterization studies. No phenotypic difference between the wild type and *ack1Δ* strains were observed. A plasmid designed for use in complementation studies was constructed but not utilized due to the absence of phenotypic variation. Several strains containing *mCherry*-tagged *ACK1* were created and initial PCRs of the 5' and 3' ends suggest proper placement of the *ACK1-mCherry* cassette within the *C. neoformans* genome. Following additional placement confirmation studies, these strains can be used to identify subcellular localization of this protein and allow purification of the endogenous protein from cell lysate that can be used for enzyme kinetic studies as well as for identifying possible interacting proteins. Further exploration is needed to elucidate acetate kinase's role in this microorganism.

1. Casadevall, A, Perfect, JR. (1998). *Cryptococcus neoformans*. Washington, DC. American Society for Microbiology.

2. Park, BJ, Wannemuehler, KA, Marston, BJ, Govender, N, Pappas, PG, Chiller, TM. (2009). Estimation of the Current Global Burden of Cryptococcal Meningitis Among Persons Living With HIV/AIDS. AIDS. 23(4): 525-530.

INTRODUCTION

Cryptococcus neoformans

Cryptococcus neoformans is a small haploid, single-celled, spherical yeast belonging in the phylum Basidiomycota. This fungus is most commonly encountered as budding yeast, its vegetative state (Hull and Heitman 2002), however under certain nutrient deprivation, these cells can sexually reproduce if both mating types, mat a and mat α, are present (Hull and Heitman 2002). This union results in the formation of filaments at the end of which basidia, containing basidiospores are produced. Under adequate conditions, the basidiospores can grow into vegetative yeast cells (Hull and Heitman 2002). Environmental and clinical strains of *C. neoformans* have shown to be of predominantly the α mating type arguing against sexual reproduction being a common practice. In 1996, Wickes et al. described similar filamentation resulting in the formation of basidiospores occurring in mat α strains in the absence of the mat a mating type (Wickes et al. 1996). This phenomenon, haploid or monokaryotic fruiting, has now become the most reasonable explanation for the presence of basidiospores in an organism found predominantly as one mating type (Hull and Heitman 2002).

C. neoformans is an environmental microorganism that is found globally in soil and has been commonly associated with pigeon feces and other bird excreta (Casadevall and Perfect 1998). The presence of yeast cells and basidiospores in the environment does not usually present a problem for most people with healthy immune systems. While it is considered an opportunistic pathogen, cases of cryptococcosis in patients with no known immune deficiencies have been documented in China (Chen et al. 2008), and

infections involving immunocompetent individuals by a related species (*C. gattii*) were reported in the Pacific Northwest (Datta 2009).

Cryptococcosis

The first documented clinical case of cryptococcosis occurred in 1894 in Germany and the first environmental isolate of *C. neoformans* was discovered in Italy that same year. It is believed that elevated awareness about the pathogen has led to more numerous and definitive diagnoses of the disease. Following the explosion of the AIDS epidemic in the early 1980s, the number of cryptococcosis cases rose abruptly (Casadevall and Perfect 1998). A study published in 2009 by Park et al. estimated the number of cryptococcal meningoencephalitis cases annually to be approximately 957,900 with about 624,700 resulting in death. Most of these cases occurred in underdeveloped nations, especially sub-Saharan Africa where access to antiretroviral agents for AIDS/HIV patients is minimal (Park et al. 2009).

C. neoformans most commonly enters its host through the respiratory system resulting in lung masses, however it can manifest itself as a primary skin lesion caused by introduction through broken skin, skin lesions secondary to internal infection, and can cross the blood-brain barrier leading to meningoencephalitis (Neuville 2003). It is not known whether aerosolized desiccated yeast cells or basidiospores that are produced by the organism are to blame for infection however due to their size and their ability to withstand desiccation and nutrient deprivation, basidiospores are most commonly thought to be the infecting agent (Wickes et al. 1996). By comparing clinical and geographical isolates of *C. neoformans*, it was demonstrated that the organism can remain dormant within its host for an extended period of time. If the host's immune system weakens, the

yeast can begin multiplying resulting in disease (Garcia-Hermoso et al. 1999). The amount of time that *C. neoformans* can remain dormant, however, remains unknown.

The pathogenicity of *C. neoformans* can be attributed to the characteristics that contribute to its virulence including its ability to synthesize a polysaccharide capsule, to produce melanin, to tolerate environmental stressors such as warm temperatures, and oxidative and nitrosative stressors. The most notable virulence is its ability to produce a polysaccharide capsule. The capsule provides protection for the cell from desiccation, masks proteins located on the cell wall that could signal the host's immune system to the presence of the pathogen, and it can make phagocytosis mechanically challenging (McQuiston and Del Poeta 2011, Zaragoza et al. 2009). The cell's ability to produce melanin is another important virulence factor. In addition to helping protect the cell from harmful environmental conditions such as exposure to UV light, components of melanin are believed to help aid in the organism's ability to withstand oxidative and nitrosative stress that is encountered upon engulfment by the phagocytic cells of the immune system (Wang and Casadevall 1994). The cell's ability to withstand the relatively warm internal human body temperature of 37˚C is also considered a virulence factor.

Treatments for Cryptococcosis

At this time, there are limited chemotherapeutic agents that are effective against this environmental opportunistic pathogen. Combinations of amphotericin B, fluconazole, and 5-flucytosine are the most commonly used drugs used to treat cryptococcosis; however, certain combinations of these drugs can result in kidney toxicities and drug resistance to 5-flucytosine when used as a sole therapeutic agent has been reported (Saag et al. 2000). Additionally, while only a few clinical strains in Africa

have demonstrated resistance to fluconazole, long-term antifungal drug regimens, commonly used to combat cryptococcosis as well as other opportunistic fungal infections have raised concerns over antifungal drug resistance and have prompted monitoring of such (Govender et al. 2011). Newer drugs and alternative therapies including the use of monoclonal antibodies have demonstrated favorable laboratory results but little clinical data is available (Pappas 2011).

It has been suggested that targeting metabolic pathways that affect survival or virulence of a pathogen might be a more effective way to eradicate the pathogen (Casadevall and Perfect 1998). One such pathway is the calcineurin signaling pathway. The calcineurin pathway plays many roles in *C. neoformans* including inducing responses to changes in the environment that affect its virulence such as heat tolerance and cell wall synthesis, and it is believed to be responsible for drug tolerance to a class of antifungal medications used for *C. albicans* (Fox et al. 2011). Cyclosporin A, a drug that inhibits signaling of this pathway has demonstrated growth inhibition in *C. neoformans* and *C. gattii* (Mody et al. 1988 and Chen et al. 2013). While the identification of enzymes and/or pathways utilized by pathogens provide potential targets for drug therapy, enzymes or pathways utilized by pathogens but not their hosts have the potential benefit of treating the disease while minimally affecting the host.

Acetate Kinase

The rapidly increasing number of sequenced genomes and search tools such as BLAST (Basic Local Alignment Search Tool) have enabled the identification of homologous proteins utilized by other organisms so that we can use what has been learned from well-studied organisms, such as *E. coli*, to try to better understand their role in other organisms. In 2006, Ingram-Smith et al. described the discovery of a putative homologous protein acetate kinase (AK), an enzyme whose role in bacteria and in the *Methanosarcina* genus of Archaea has been well studied, in *C. neoformans* (Ingram-Smith et al. 2006). In addition to sequence similarities identified in a BLAST query, amino acids that make up the phosphoryl donor/acceptor (ATP/ADP) binding sites as well as residues that make up the acetate binding pocket of AK in *M. thermophila* are conserved in *C. neoformans* (Ingram-Smith et al. 2006; Thaker et al. 2013). Putative homologs of AK have been identified in other lower eukaryotic organisms, some of which are pathogenic including *Entamoeba histolytica* and *Aspergillus fumigatus* (Bragg and Reeves 1962; Ingram-Smith et al. 2006). Interestingly, no homologs have, as yet, been found in humans or other higher eukaryotes suggesting the presence of a unique pathway that could be targeted by chemotherapeutic agents (Ingram-Smith et al. 2006).

In bacteria, acetate kinase is an enzyme that is part of the glyoxylate pathway that is responsible for the assimilation of acetate from excess acetyl-CoA, an important metabolic intermediate (Ingram-Smith et al. 2006). During aerobic respiration and under high glucose concentrations, the production of acetyl-CoA exceeds the amount that the cell can utilize for important metabolic processes such as the energy generating tricarboxylic acid cycle and fatty acid biosynthesis (Wolfe 2005). As a result, excess

acetyl-CoA is converted into acetate through a reversible acetate assimilation pathway in which excess Acetyl-CoA is converted into acetyl-phosphate by the enzyme phosphotransacetylase (PTA). An inorganic phosphate is transferred from acetyl phosphate to ADP to produce the high-energy molecule ATP and acetate (Wolfe 2005). The acetate produced is then excreted the acetate from the cell. When carbon stores become depleted, the acetate is actively transported into the cell and converted back into acetyl-CoA by the enzyme acetyl-CoA synthetase (ACS) (Wolfe 2005).

In *C. neoformans*, however, specifics of the glyoxylate pathway have not yet been elucidated. According to Ingram-Smith et al. (2006), one striking difference between the pathway in *E. coli* and that in *C. neoformans* is the absence of a phosphotransacetylase (PTA) homolog, the enzyme responsible for producing the substrate, acetyl-phosphate, in *C. neoformans.* This absence led Drs. Kerry Smith and Cheryl Ingram-Smith, our collaborators at Clemson University, to suggest that this PTA pathway is not used to synthesize the acetate precursor. Instead, the Smith lab has identified two homologs (XFP1p and XFP2p) of an enzyme previously thought to be present only in bacteria, xylulose 5-phosphate/fructose 6-phosphate phosphoketolase, XFP. In bacteria, XFP catalyzes a reaction that breaks down D-xylulose 5-phosphate or D-fructose 6-phosphate to produce acetyl-phosphate (Meile et al. 2001). Interestingly, the gene that codes for this enzyme has been closely linked to genes that code for PTA and/or AK in several bacteria (Meile et al. 2001).

Reverse Genetics

One manner in which information about the function of specific proteins and their role(s) in various organisms can be gained is through reverse genetics studies. This approach involves identification of putative homologous proteins using programs such as BLAST (Basic Local Alignment Search Tool). These programs search genome sequence databases for nucleotide or amino acid sequence similarities to a gene or protein of interest. Once one is identified, the DNA sequence data can be used to produce mutant strains in which the protein of interest is rendered nonfunctional by introducing mutations within gene, deleting the gene from the genome, or by performing RNA interference (RNAi) in which small gene sequences are used to induce destruction of mRNA containing the same sequence. Once the gene is disrupted, the mutant organism is subjected to different environmental conditions and its phenotypic response observed and compared to that of the normal, wild type (WT) organism. If a difference in phenotype is revealed, complementation is performed to induce normal gene function in an attempt to restore the WT phenotype. Information gained by identifying conditions that elicit a different phenotype increase the understanding about its role in the organism.

Creation of *ack1Δ* strains

To learn more about the role AK plays in *C. neoformans*, this reverse genetics study was initiated. Dr. Indrani Bose created fourteen strains in which the gene encoding acetate kinase, *ACK1*, was deleted. The construct that was used to create the mutant strains contained three parts: the 5' untranslated region upstream of *ACK1*, a neomycin resistance gene (NEO^R), and the 3' untranslated region. This construct that was used to was produced using overlap PCR of the three fragments listed above as the template.

Once the entire construct was confirmed, it was PCR amplified, coated onto gold beads and shot into KN99 *C. neoformans* cells (WT) using a gene gun. Cells that underwent homologous recombination and successfully integrated the construct into their genome, replacing *ACK1* with NEO^R, were able to grow in the presence of neomycin. Genomic DNA extractions were performed on the colonies that arose on the neomycin plates and used as the template for PCRs to test for the presence of the construct within the genome. Fourteen strains demonstrated amplification of a portion of NEO^R.

In order to ensure the complete and clean deletion of *ACK1*, further confirmation studies were performed. A cDNA analysis was used to ensure that mRNA coding for AK was not being produced in the *ack1Δ* stains, and a Southern blot using probes for *ACK1* and NEO^R was performed to demonstrate that a single integration of NEO^R had occurred and that *ACK1* had been removed from the genome. It is important to demonstrate that proper placement of the NEO^R to ensure that it had not integrated randomly resulting in the disruption of another gene. These microbes were then used in a number of experiments to observe the phenotypes the cells exhibit under a variety of conditions to try to reveal a difference in phenotype between the *ack1Δ* strains and the WT strain (KN99) that will offer a clue as to the role AK plays in *C. neoformans*. It was thought that a starting place would be to test the *ack1Δ* strain's carbon source utilization abilities since AK is utilized in *E. coli* to deal with excess acetyl-CoA in high glucose condition. The other phenotypes tested in this study involve virulence factor characteristics of the pathogen including polysaccharide capsule synthesis, melanization, temperature tolerance, tolerance to hypoxic, nitrosative, and oxidative stressors among others because a defect in any of these abilities could possibly attenuate the pathogen. A plasmid

containing *ACK1* was constructed for complementation studies in the event a unique phenotype was observed. Finally, five *C. neoformans* strains were created in which *ACK1* is tagged with the red fluorescent protein, mCherry, which can be used for subcellular localization of acetate kinase within the cell. It can also be used to purify AK from cell lysate using antibodies against mCherry. The purified protein can then be used for enzyme activity assays.

Significance

The motivation behind this reverse genetics study is to characterize the phenotype of *Cryptococcus neoformans* mutants lacking the acetate kinase gene (*ACK1*) in hopes that it will broaden our understanding of how the expression of *ACK1* affects cell function. It is hopeful that this information will help elucidate the metabolic pathway of which AK is believed to play a role. By gaining a thorough understanding of important metabolic pathways including intermediate substrates and enzymes, especially ones that are unique to pathogenic organisms, potential targets for chemotherapeutic agents may be identified. To date, the gene that encodes this enzyme has not been characterized in *C. neoformans*. It is this gap in the literature was the driving force behind this reverse genetics study.

MATERIALS AND METHODS

cDNA Analysis for *ack1Δ* Strain Confirmation

Total RNA was extracted from 3 ml overnight cultures grown in YPD (1% (w/v) yeast extract, 2% (w/v) peptone, and 2% (w/v) dextrose) at 30˚C using the Trizol method. The cells were centrifuged using an Eppendorf 5801R centrifuge rotor FA-45-30-11 at 956 x g for 5 minutes at 4˚C. The cells were bead beaten at room temperature (RT) in 750µl of TRIzol® 8 times (1 min beating followed by 2 min incubation on ice). The lysate was incubated for 10 minutes at room temperature (RT), treated with 1/5th chloroform, incubated at RT for 5 min, and centrifuged at 15,294 x g for 15 minutes at 4˚C. An equal volume of isopropanol was added to the supernatant, incubated at 10 min at RT, and centrifuged at 15,294 x g for 10 min at 4˚C. The pellets were washed in 70% ethanol, air dried, and resuspended in 40 µl of diethylpyrocarbonate (DEPC)-treated water. RNA was precipitated using 7.5 M LiCl to a final concentration of 2.5 M and incubating overnight at -20˚C. The RNA was pelleted by centrifugation at 20,817 x g for 20 min at 4˚C. The pellets were washed twice in 70% ethanol, air dried, resuspended in 50 µl of DEPC water, and quantitated on a Nanodrop 1000. 0.5 µg of total RNA was used in a 20 µl reaction to synthesize cDNA using the Thermo Scientific Verso™ cDNA Synthesis Kit (Cat no: AB-1453/A and Lot no: 0612/17).

Amplification of *ACK1* cDNA (using primers KIO25 and KIO26) and *ACT1* cDNA (using primers BLO01 and BLO02) in the same reaction was performed (see Appendix A for a list of primers). Each reaction was performed in a final volume of about 50 µl using 3 µl cDNA template from the above procedure with 10x PCR buffer

and Taq polymerase. A cycle consisting of 94˚C for 30 sec, 30 cycles of 94˚C for 30 sec followed by annealing at 60˚C for 30 sec and extension at 72˚C for 1.5 min, and a final extension of 5 min was used for this amplification. A 0.8% (w/v) TBE-agarose gel was used for visualization.

All DNA agarose gels were made with TAE buffer (Tris-acetate-EDTA) or TBE buffer (Tris-borate-EDTA) containing 0.05 μl/ml of ethidium bromide for visualization. The gels were 0.8% (w/v) in concentration unless noted otherwise.

Southern Blot Analysis for *ack1Δ* Strain Confirmation

Amplification of *ACK1* probe (using primers KIO21 and KIO22) was performed in a 50 μl reaction on a cycle consisting of 98˚C for 30 sec, 30 cycles of 98˚C for 10 sec, annealing at 54˚ for 15 sec and a 17 sec extension at 72˚C, and a final 5 min extension at 72˚C. Amplification of the NEO^R probe (using primers KIO23 and KIO24) was performed in 50 μl reactions on a cycle consisting of 98˚C for 30 sec, 30 cycles of 98˚C for 10 sec, annealing at 59˚ for 15 sec and a 26 sec extension at 72˚C, and a final 5 min extension at 72˚C. 5 μl of each probe were visualized using a 0.8% TBE-agarose gel. The probe DNA was purified using the Promega Wizard® SV Gel and PCR Clean-Up System and eluted in 50 μl of the provided nuclease-free water. 5 μl of each sample was run on a 0.8% TAE-agarose gel for visualization and 0.2 μl was quantified on a Nanodrop 1000. 100 ng of probe DNA was used to prepare the probe using Amersham Gene Images™ AlkPhos Direct™ Labeling and Detection kit.

Two sets of *Xho*I (NEB) and *Spe*I (NEB) restriction digests were performed, each containing 10 μl of gDNA using 10x BSA (NEB) and Buffer 4 (NEB) in 35 μl reactions.

The digests were incubated 27 hours at 37˚C. Fifteen μl of each sample was run on a 0.8% TAE-agarose gel and visualized.

The gel was soaked depurination buffer (11 ml HCl in 989 ml DI H_2O) for 10 min with gentle agitation, rinsed in DI water, soaked in denaturation buffer (87.66 g NaCl and 20 g NaOH in 1L) for 30 min with gentle agitation, rinsed, and soaked in neutralization buffer (87.66 g NaCl and 60.5 g Tris base in 1L with pH adjusted to 7.5), 30 minutes with gentle agitation, and rinsed.

The DNA was transferred onto the Amersham Hybond™-N^+ nylon transfer membrane with 1X nucleic acid transfer buffer (4.41 g Tri-sodium citrate and 8.77 g NaCl in 1 L pH adjusted to 7.8). The membrane was dried for 2 hrs at 80˚C.

100 ng of *ACK1* and *NEO*^{R} probe were used in separate probe hybridization reactions each containing 10 ml of pre-warmed hybridization buffer (0.5 M NaCl and 4% (w/v) blocking reagent added to kit-supplied hybridization buffer). The tubes were allowed to incubate overnight at 55˚C.

Following overnight hybridization, each blot was washed twice in preheated primary wash solution (120 g urea, 1 g SDS, 100 ml of 0.5 M sodium phosphate pH 7.0, 8.7 g NaCl, 1 ml of 1.0 M $MgCl_2$, and 2 g blocking reagent (supplied in kit) in 1 L) for 10 min at 55˚C with gentle agitation and washed twice in 125 ml of 1x secondary wash solution (12.5 ml of a 20X secondary wash solution (121 g Tris base and 112 g NaCl in 1L) and 237.5 ml of DI water, and 500 μl of 1M $MgCl_2$) for 5 min at RT. The excess wash buffer was drained from the blot, 2 ml of CDP Star was applied to each blot, and incubated for 5 min at RT. The blots were wrapped and exposed to autoradiography film for approx 1 hr and the film was manually developed.

Phenotype Characterization Studies

Carbon Source Utilization:

Petri plates containing media for testing the utilization of carbon sources were prepared (6.8 g/L Difco yeast nitrogen base (YNB) without amino acids and 18 g/L of agar). Glucose, galactose, sucrose, sorbitol, ethanol, glycerol, and D-xylose were added to separate batches of medium in 2% and 0.2% concentrations, and sodium acetate was added to the medium in 0.25%, 0.5%, and 2% concentrations. The plates were inoculated with KN99 mat α and a variety of *ack1Δ* strains and incubated at 30˚C for at least three days.

Temperature Sensitivity:

YPD plates (YPD (50 g/L), and agar (18g/L) were streaked with KN99 mat α and a variety of *ack1Δ* strains. The plates were incubated at room temperature (RT), 30˚C, 37 ˚C, and 40˚C for at least 3 days.

Melanin Production:

Niger seed agar plates (niger seed (70 g/L), glucose (2%), and agar (20 g/L) (Griffith 2012) were inoculated with KN99 mat α and a variety of *ack1Δ* strains in a circular manner. The plates were placed in the dark and incubated at RT until melanin was observed (Griffith 2012).

Nitrosative Stress:

Nitrosative stress plates (YNB without amino acids (6.8 g/L), agar (18 g/L), and 0.1 M $NaNO_2$ (7.5 ml/L)) were streaked KN99 mat α and a variety of *ack1Δ* strains and incubated at 30˚C for at least three days.

Hypoxia-Mimicking Conditions Using $CoCl_2$:

The 0.7 mM, 0.53 mM, and 0.25 mM $CoCl_2$ plates (YNB without amino acids (6.8 g/L) and agar (18 g/L), and 0.1M $CoCl_2$) were inoculated with KN99 mat α and a variety of *ack1Δ* strains were streaked onto the plate, and the plate was incubated at 30˚C for at least three days (Ingavale et al. 2008).

pH:

The pH plates (YPD (50 g/L), agar (18 g/L) adjusted to pH 5, pH 7, pH 9, and pH 11 using NaOH or HCl) were streaked with KN99 mat α and a variety of *ack1Δ* strains and incubated at 30˚C for at least three days.

Filamentation Following Sexual Reproduction:

Each of the *ack1Δ* strains were mixed with KN99 mat a and KN99 mata α separately on YPD (50 g/L) and incubated overnight at 30˚C. Mating plates (1X Murashige-Skoog Basal Salt Mixture and agar (17 g/L) to pH 5.7) were streaked with each sample and allowed to incubate in the dark at RT until filamentation was observed. The filamentation was photographed using a Leica $MZ12_5$ microscope in Dr. Pechmann's lab.

Oxidative Stress Using H_2O_2:

The 0.75 mM, 0.5 mM, and 0.25 mM oxidative stress plates (YNB without amino acids (6.8 g/L), agar (18 g/L), pH 7, and 0.1M H_2O_2) were streaked with KN99 mat α and a variety of *ack1Δ* strains and incubated at 30˚C for at least three days.

Cluster Growth Phenotype:

YPD broth (5 ml) and minimal medium broth (5 ml) were inoculated with KN99 mat α and a variety of *ack1Δ* strains and incubated overnight at 30˚C. Nikon Microphot-FXA microscope was used for documentation.

Capsule Formation:

KN99 mat α and a variety of ack1Δ strains were incubated at 30˚C in 10 ml Sabouraud medium (1% (w/v) peptone, 4% (w/v) dextrose in DI H_2O) for approximately 20 hours with moderate shaking. One ml of each sample was centrifuged at 14,000 x g for 5 minutes, washed twice in 500 μl of 1X PBS (NaCl (137 mM), KCl (2.7), KH_2PO_4 (1.5 mM), and Na_2HPO_4 (8.5 mM)), and centrifuged at 14,000 x g for 5 minutes. The cells were resuspended in 200 μl of capsule-inducing medium (1/10 Sabouraud in 50 mM pH 7.3 MOPS) and transferred to 10 ml of capsule-inducing medium. The cells were incubated for approx. 18 hours at 37˚C with moderate shaking (Zaragoza and Casadevall 2004). The cells were observed and photographed using a microscope at Clemson University and a Nikon Microphot-FXA microscope.

Cell Wall Integrity:

Cell wall integrity plates (YPD (50 g/L), agar (18 g/L), and Congo Red stain (5 ml/L) or 10% SDS (1 ml/L) were streaked with KN99 mat α and a variety of *ack1Δ* strains and incubated at 30˚C for at least three days.

***ACK1* Complementation Plasmid for Electroporation**

Genomic DNA was extracted from 3 ml of overnight cultures grown in YPD (50 g/L) at 30˚C. The cells were centrifuged using a table top centrifuge at 14,000 x g, resuspended in 500 µl of extraction buffer (50 mM TRis-HCl (pH 8.0), 20 mM EDTA, and 1% SDS), bead beaten using a vortexer at 5 min intervals followed by 1 min ice incubation until 50-80% of cells lysed, and incubated at 70˚C for 10 min. Five molar potassium acetate (200 µl) and 5 M NaCl (150 µl) were added to each tube, mixed, incubated on ice for 20 minutes, and centrifuged at 14,00 x g at RT for 10 minutes and the supernatant was transferred to new tubes. Chloroform (450 µl) was added to the supernatant, mixed, and centrifuged at 14,000 x g at RT for 10 minutes. The aqueous phase (top phase) was transferred to new tubes. Twenty µl of 30% PEG8000 was added to the aqueous phase and centrifuged at 14,000 x g for 10 minutes. The pellet was resuspended in 50 µl of H_2O, 1 µl of RNase (500 µg/ml) added, and incubated in a 37˚C water bath for 30 minutes. A tenth of a volume of 3 M sodium acetate (5 µl) and 3 volumes of 100% ethanol (150 µl) were added, incubated at -20˚C at least 30 min, and centrifuged at 4˚C on 14,000 x g for 10 minutes. The pellet was resuspended in 50 µl of H_2O (Bose 2009).

A 50 µl PCR (BLO11 and BLO12) using 5X Phusion® HF Reaction Buffer, Phusion® *Taq* Polymerase, and 1.0 µl of template DNA (KN99 mat α) was run on a cycle consisting of 30 sec at 98˚C, 30 cycles of 98˚C, annealing at 61˚C for 15 sec, and a 2 min extension at 72˚C, and a final 5 min extension at 72˚C. The PCR products were purified using Qiagen® QIAquick® PCR Purification Kit. Five µl was visualized on a 0.8% TBE-agarose gel.

A miniprep of pHYG7-KB1 vector using 3 ml of overnights grown in LB + ampicillin (100 mg/ml) was performed using Qiagen® QIAprep® Spin Miniprep Kit. The DNA was eluted in H_2O (50 µl) and stored at -20˚C.

*Spe*I (NEB) digest of the purified *ACK1* PCR (15 µl) and pHYG7-KB1 (15 µl) were digested using Buffer 4 (NEB), 10x BSA (NEB) in 60 µl reactions. The tubes were incubated overnight at 37˚C. *Spe*I was inactivated via incubation at 80˚C for 20 min.

1 µl of NEB CIP (calf intestinal alkaline phophatase) was added to the *Spe*I-digested pHYG7-KB1 vector and incubated at 37˚C for 1 hr.

An ethanol precipitation was performed using one-tenth volume (6 µl) of 3 M sodium acetate and 3 volumes (180 µl) of 100% ethanol to each digest. They were incubated overnight, and centrifuged at 4˚C for 30 minutes. Seventy percent ethanol (200 µl) was added and the pellets, centrifuged at 4˚C for 15 min, and air-dried. The DNA was resuspended in 40 µl of H_2O. One half µl of each was visualized on a 0.8% TBE-agarose gel with ethidium bromide for visualization.

ACK1 (6 µl) was ligated into pHYG7-KB1 (2 µl) in a 20 µl reaction containing T4 DNA ligase buffer and T4 DNA ligase. The reaction was incubated at 16˚C for 36 hours.

Competent *E. coli* cells were chemically transformed using 8 µl of linearized vector in one transformation and 8 µl of ligation reaction in a second transformation. The tubes were incubated on ice for 30 min and incubated at 37˚C for 45 seconds. SOC (250 µl) was added, the tubes incubated for 1 hour at 37˚C, plated on LB + ampicillin (100 mg/ml), and incubated overnight at 37˚C.

Colony PCRs were performed (using primers KIO21 and KIO22) using 10x PCR Buffer and Taq polymerase in 20 μl reactions. The reactions were run on a cycle of 30 sec at 94˚C, 30 cycles of 30 sec at 94 ˚C, annealing at 57˚C for 30 sec and 45-sec extension at 72˚C, and a final 5-min extension at 72˚C. Five μl of was run on a 0.8% TBE-agarose gel for visualization.

Minipreps using 3 ml of overnight cultures of colonies #2 and #7 grown in LB + amp (100 mg/ml) at 37˚C were performed using the Qiagen® QIAprep® Spin Miniprep Kit.

Three 15 μl *Xba*I digests of colonies #2 and #7 and pHYG7-KB1 vector using Buffer 4 (NEB), 10x BSA (NEB), and 3 μl of miniprep DNA and vector only were incubated overnight at 37˚C. The entire reaction was run on a TBE-0.8% agarose gel for visualization.

***ACK1-mCherry* Construct for Subcellular Localization of Acetate Kinase**

The three fragments making up the *ACK1-mCherry* construct were PCR amplified.

A 50 μl PCR of fragment #1 (using primers KIO27 and KIO28) using 5x HF Buffer, Phusion Taq polymerase, and KN99 mat α as template was run on a cycle of 30 sec at 98˚C, 30 cycles of 10 sec at 98˚C, 15 sec annealing at 63˚C, and 1 min-45 sec extension at 72˚C, and a final 6-min extension at 72˚C.

A 50 μl PCR of fragment #2 (using primers KIO29 and KIO30) using 5x HF Buffer, Phusion Taq polymerase, and pLKB25 (containing *mCherry-NEO*^{R}) as template was run on a cycle of 30 sec at 98˚C, 30 cycles of 10 sec at 98˚C, 15 sec annealing at 65˚C, and 1 min-45 sec extension at 72˚C, and a final 6-min extension at 72˚C.

A 50 μl PCR of fragment #3 (using primers KIO31 and KIO32) using 5x HF Buffer, Phusion Taq polymerase, and KN99 mat α as template was run on a cycle of 30 sec at 98˚C, 30 cycles of 10 sec at 98˚C, 15 sec annealing at 60˚C, and 1 min extension at 72˚C, and a final 5-min extension at 72˚C.

Fragments #1 and #3 were PCR purified using the Qiagen® QIAquick® PCR Purification Kit. Fragment #2 was cut from the gel and purified using the Qiagen® QIAquick® Gel Purification Kit. The fragments were eluted in 50 μl of H_2O. Five μl of each was run on a 0.8% TBE-agarose gel for visualization.

Fragment #1 digested with *Spe*I in a 60 μl reaction containing Buffer 4 (NEB), 10x BSA (NEB) and 12 μl of fragment #1 for 4 hrs at 37˚C, incubated at 80˚C for 20 minutes, then digested with *Bam*HI (NEB) at 37˚C for 4 hrs. The digest was purified using the QIAquick® PCR Purification Kit and eluted in 50 μl of H_2O.

Fragment #2 was digested with *Spe*I and *Nde*I in a 60 ml reaction containing Buffer 4 (NEB), 10x BSA (NEB) and 20 μl of fragment #2, incubated 37˚C for 4 hrs then purified using the QIAquick® PCR Purification Kit. The DNA was eluted in 35 μl of H_2O.

Fragment #3 was digested with *Nde*I (NEB) in a 60 μl reaction using Buffer 4 (NEB), 10x BSA (NEB), and 12 μl of fragment #3, incubated at 37˚C for 4 hrs. The digest was PCR purified using the QIAquick® PCR Purification Kit, and the DNA was eluted in 30 μl of H_2O. A second 60 μl *Kpn*I digest was performed using Buffer 1 (NEB), 10x BSA (NEB), and all of the purified *Nde*I-digested fragment #3, incubated at 37˚C for 4 hrs, purified using the QIAquick® PCR Purification Kit, and eluted in 50 μl of H_2O.

The vector, pCR2.1 Topo, was digested with *Bam*HI using Buffer 4 (NEB), 10x BSA (NEB), and 12 μl of the vector, incubated at 37˚C for 4 hrs, PCR purified using the QIAquick® PCR Purification Kit, eluted in 30 μl of H_2O. A second digest was performed in a 60 μl reaction using Buffer 1 (BSA), 10x BSA (NEB), and 30 μl of purified *Bam*HI-digested vector, incubated at 37˚C 4 hours, PCR purified using the QIAquick® PCR Purification Kit, and eluted inn 50 μl of H_2O.

Five μl of each of the three fragments and the vector were separated on a 0.8% TBE-agarose gel for visualization and relative concentration determination.

Two ligation reactions of the *ACK1-mCherry* construct were performed, one using T4 DNA ligase buffer, 1 μl of vector, 1 μl of fragment #1, 3 μl of fragment #2, 0.5 μl of fragment #3, and T4 DNA ligase, and the other reaction using T4 DNA ligase buffer, 1 μl of vector, 2 μl fragment #1, 6 μl of fragment #2, 1 μl of fragment #3, and T4 DNA ligase. The reactions were incubated overnight at 16˚C.

Transformation of the 4 μl of each ligation reaction into competent *E. coli* cells was performed as described above and colony PCRs on the transformants were done using the primers KIO21 and KIO22, 10x PCR Buffer, and Taq polymerase. The PCRs were run on a cycle consisting of a 30 sec at 94˚C, 30 cycles of 30 sec at 94˚C, a 30 sec annealing step at 59˚C and a 45 sec extension step at 72˚C, and a final 5 min extension step at 72˚C. Five μl of each reaction was run on a 0.8% TBE-agarose gel for visualization.

Minipreps were performed using the Qiagen® QIAprep® Spin Miniprep Kit on colonies A8, B6, B7, B10, and B11. *Xho*I restriction digests (15 μl) were performed

using Buffer 4 (NEB), 10x BSA (NEB), and 3 μl of plasmid DNA, incubated overnight at 37˚C, and run on a 0.8% TBE-agarose gel for visualization.

Four 50 μl PCRs in which only the annealing temp was varied were performed in preparation for biolistic transformation using primers KIO27 and KIO32, 5X HF Buffer, Phusion Taq polymerase, and 1 μl of the colony A8 miniprep DNA. The reaction was run on a program consisting of 10 sec at 98˚C, 30 cycles of 10 sec at 98˚C, 10 sec annealing steps at 62˚C, 63˚C, 63.5˚C, and 64˚C, and a 3 min extension step at 72˚C, and a final 5 min extension step at 72 ˚C. The PCR products were purified using the QIAquick® PCR Purification Kit and eluted in 30 μl of H_2O. One μl of each sample was run on a 0.8% TBE-agarose gel for visualization.

Six biolistic transformations of KN99 mat α cells with the *ACK1-mCherry* constructs were performed by Dr. Bose at Washington University in St. Louis, Missouri. The six transformation reactions were plated on YPD + G418 plates and mailed back to WCU to confirm the presence and placement of the entire *ACK1-mCherry* construct.

Genomic DNA extractions, as described above, were performed on the transformants and confirmation 20 μl PCRs of the 5' and 3' ends of the construct were performed. The PCRs consisted of 5X HF Buffer, primers KIO33 and BLO45 for the 5' end confirmation and primers BLO46 and KIO12 for the 3' end confirmation, Phusion Taq polymerase, and 3.0 μl of gDNA. The 5' end PCRs were run on a program consisting of 30 cycles that included a 10-second denaturation step at 98˚C, a 30-second annealing step at 56˚C, and a 1-minute, 40-second extension step at 72˚C, and the 3' end PCRs were run on a program that consisted of 30 cycles that included a 10-second denaturation step at 98˚C, a 30-second annealing step at 63˚C, and a 1-minute, 15-second

extension step at 72˚C. Both programs included an initial 10-second denaturation step at 98˚C and a final 5-minute extension step at 72˚C. Five μl of each reaction were run on a 0.8% TAE-agarose gel for visualization.

RESULTS AND DISCUSSION

cDNA Analysis for *ack1Δ* Strain Verification

cDNA analysis was performed to confirm that the *ack1Δ* strains are not producing mRNA coding for Ack1p. To demonstrate the presence of template DNA in each sample, amplification of an actin gene, *ACT1*, was performed in the same PCR reaction. *ACT1* is expressed continuously so amplification is expected in the presence of cDNA. The primers designed for this experiment consisted of two separate exonic sequences from *ACK1*. Due to the presence of introns, this allowed for differentiation between the amplification of cDNA versus gDNA contamination based on the size of the PCR product. Amplification of cDNA was expected to yield a 1,032 bp fragment, but amplification of gDNA was expected to yield a 1,539 bp product. The same principle is true with *ACT1* PCR with the gDNA yielding a 900 bp product and the cDNA yielding an 810 bp product.

PCR to verify the *ack1Δ* strains yielded two amplified products in the WT gDNA sample measure approximately 9 Kb and 1.5 Kb (Figure 1). The larger band corresponds in size to the expected product length (1,539 bp) resulting from a PCR using the *ACK1* primers KIO25 and KIO26 and WT gDNA as the template. The smaller band corresponds to the expected product size (900 bp) resulting from amplification of a portion of the actin gene *ACT1* using the primers BLO1 and BLO2 and WT gDNA as the template.

The two bands in the WT cDNA samples are smaller than those seen in the WT gDNA sample due to the absence of introns in the cDNA. The bands on the gel of the

KN99 mat α cDNA sample correspond with these expected fragment lengths (1,032 bp and 810 bp) demonstrating the presence of both *ACK1* mRNA and *ACT1* mRNA in the sample.

A single band corresponding to the size of the *ACT1* fragment amplified from WT cDNA is noted in all the *ack1Δ* strains demonstrating the presence of *ACT1* mRNA in the samples, however no amplification of *ACK1* mRNA is demonstrated in any of the *ack1Δ* strains. These findings help support the initial PCR findings that the *ACK1* deletion was successful.

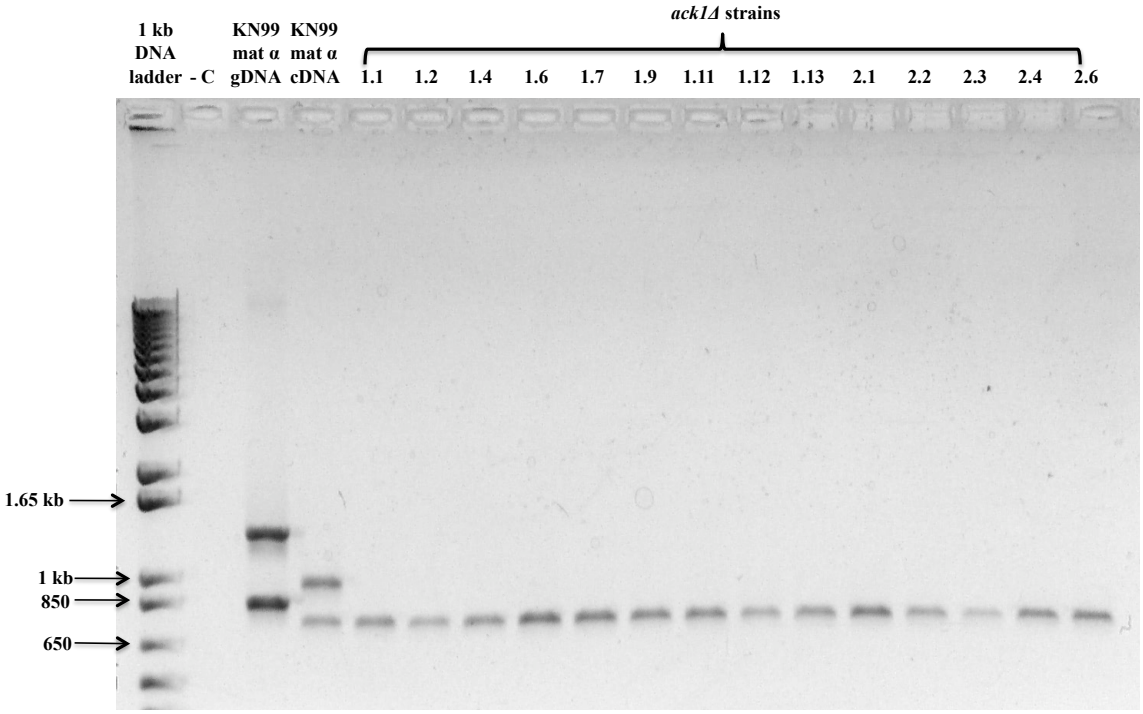

Figure 1: PCR Products of cDNA Analysis to Confirm *ACK1* Deletion. PCR products of amplification of *ACK1* and *ACT1* from gDNA of KN99 mat α (WT), cDNA from the WT, and all of the *ack1Δ* strains.

Southern Blot Analysis for *ack1Δ* Strain Confirmation

A Southern blot was performed to allow localization of *ACK1* and/or NEO^R sequences within gDNA samples to determine which sequences are present and to ensure that only one deletion construct containing NEO^R integrated into the *ack1Δ* strains. Autoradiography film exposure resulting from light emission from a chemiluminescent reaction of the alkaline phosphatase labeled *ACK1* and NEO^R probes following CDP Star application will allow for localization of the hybridized probes to complementary sequences within digested gDNA.

The *ACK1* and NEO^R Southern blot probes were amplified using PCR (Figure 2) and were checked for size by gel electrophoresis. The *ACK1* probe DNA seen located where we expected (519 bp) using primers KIO21 and KIO22 with WT gDNA as the template. The NEO^R probe DNA corresponds to the expected size of 801 bp resulting from amplification of *ack1Δ 1.1* gDNA as the template with primers KIO23 and KIO24.

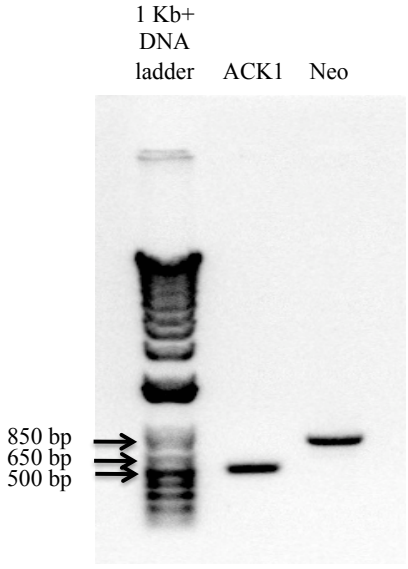

Figure 2: Southern Blot Probe DNA. 1 Kb Plus DNA ladder, purified *ACK1* probe DNA (519 bp), and NEO^R probe DNA (801 bp).

A restriction digest was performed to cut the gDNA into smaller fragments so that probe hybridization would occur on a fragment of known size that could be referenced by a 1 Kb Plus DNA ladder. *Xho*I and *Spe*I, were chosen for the gDNA digestion because these restriction sites are absent within *ACK1* as well as the *ack1Δ* construct used to create the deletion strains (Figure 3). Digestion of WT gDNA using these enzymes was anticipated to produce a 5,053 bp fragment that contains *ACK1*. The *ACK1* probe was expected to hybridize to a fragment of this size in the WT strain but not the in the *ack1Δ* strains since *ACK1* was anticipated to be absent from the WT strain. *Xho*I and *Spe*I restriction digestion of the *ack1Δ* strain gDNA was expected to produce a 6,073 bp fragment that contains NEO^R. The Southern blot using the NEO^R probe was anticipated to hybridize to an ~6 Kb fragment only in the *ack1Δ* strains. The difference in fragment size between the WT strain and the *ack1Δ* strain is due to the fact that *ACK1* is 1,661 bp in length while NEO^R is 2,681 bp in length. The distance between the *Xho*I restriction site and the 5' end of these two genes remains the same (1,720 bp) in both strains as does the distance between the 3' end of the two genes and the *Spe*I site (1,672 bp).

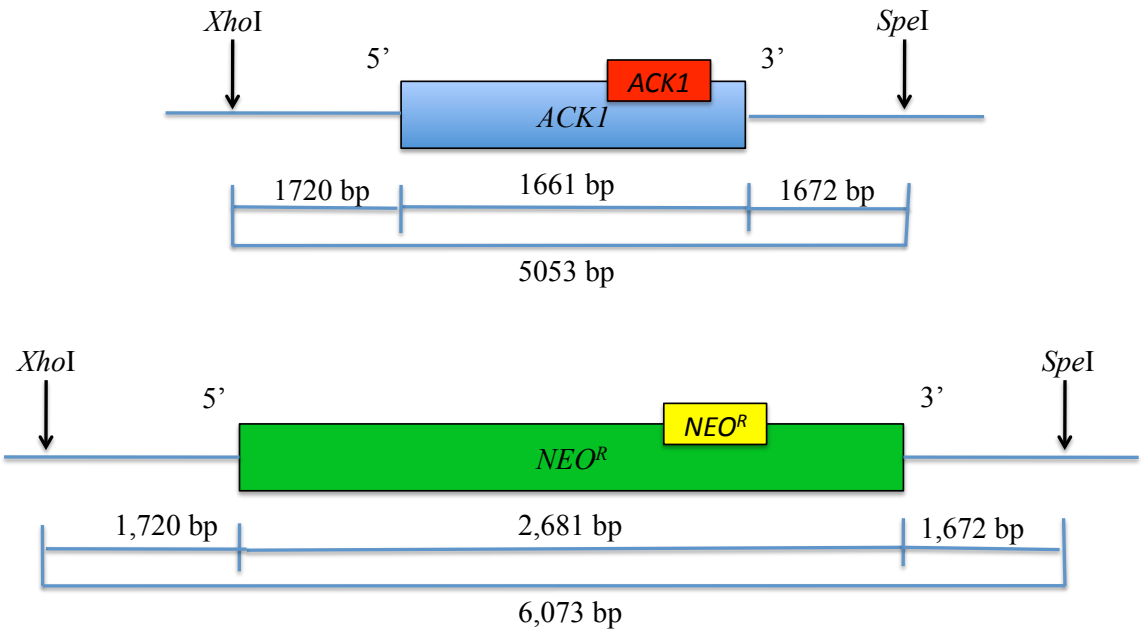

Figure 3: Diagram of *Xho*I and *Spe*I Restriction Sites for Southern Blot Digest. Hybridization of the *ACK1* probe is expected to occur on a gDNA fragment measuring approximately 5 Kb (top) and *NEO*^{R} probe is expected to hybridize to a 6 Kb fragment of gDNA (bottom).

The *Xho*I and *Spe*I digested gDNA (Figures 4 and 5) demonstrates two large dark bands of undigested WT (KN99) and *ack1Δ* 1.2 gDNA near the top of the gel, and smeared digested WT and *ack1Δ* gDNA. There are no bands noted at the top of the gel horizontal to the undigested gDNA demonstrating full digestion of the gDNA by the endonucleases. The undigested gDNA samples were used as landmarks over which the dark areas of the samples on the autoradiography film were overlaid to allow identification of the DNA fragment size to which the probe hybridized using the I Kb Plus DNA ladder.

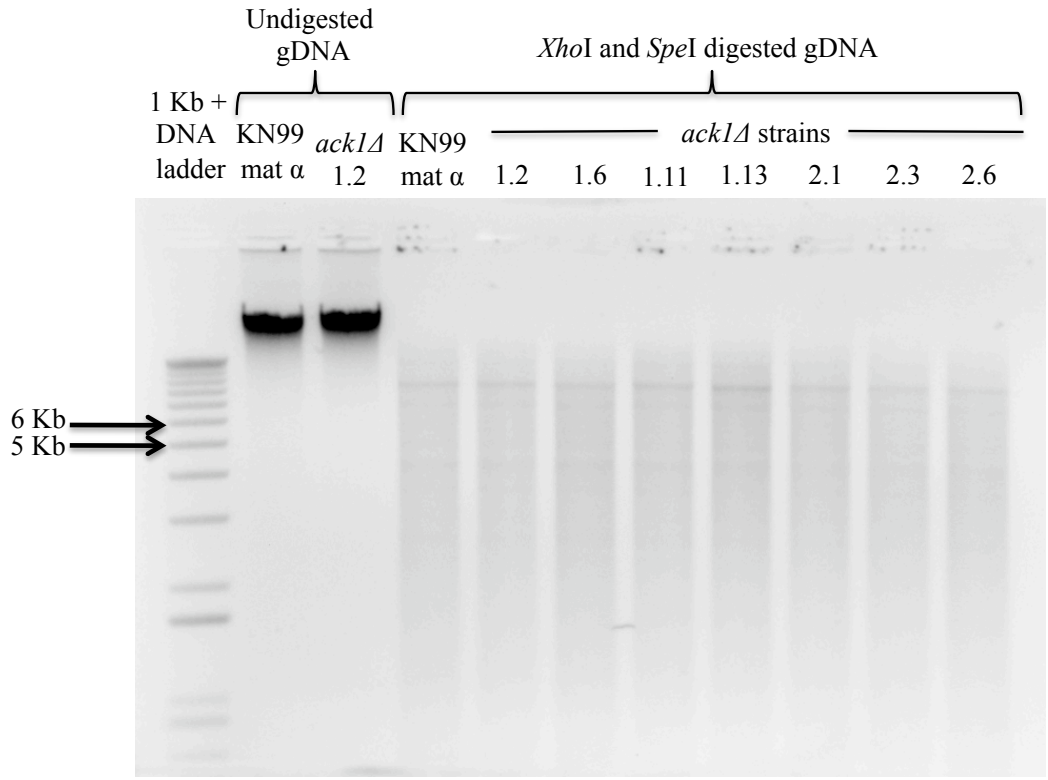

Figure 4: *Xho*I and *Spe*I Digested gDNA for *ACK1* Southern Blot. Image of 0.8% agarose gel containing 1 Kb Plus DNA ladder, undigested *ACK1* and *ack1Δ* 1.2 gDNA for orientation purposes. *Xho*I and *Spe*I digested WT, and *Xho*I and *Spe*I digested gDNA of *ack1Δ* 1.2, 1.6, 1.11, 1.13, 2.1, 2.3, and 2.6.

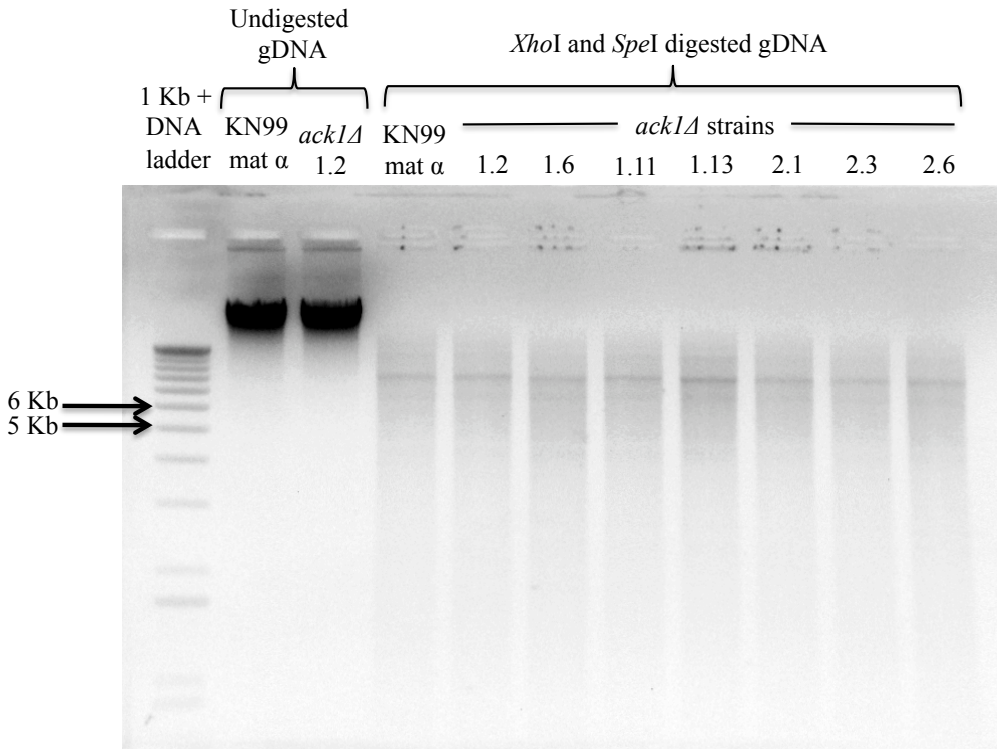

Figure 5: *Xho*I and *Spe*I Digested gDNA for *NEO*^{R} Southern Blot. Image of 0.8% agarose gel containing 1 Kb Plus DNA ladder, undigested *ACK1* and *ack1Δ* 1.2 gDNA for orientation purposes. *Xho*I and *Spe*I digested WT, and *Xho*I and *Spe*I digested gDNA of *ack1Δ* 1.2, 1.6, 1.11, 1.13, 2.1, 2.3, and 2.6.

The autoradiography film from the hybridization of the *ACK1* probe (Figure 6) demonstrates a dark band near the top of the gel in lane 2 with a less intense band at the same position in lane 3. A distinct dark band is noted in the digested WT gDNA further down the gel, but no such band is noted in the digested *ack1Δ* strain samples. Faint shadowing is also observed along the length of all of the lanes containing digested gDNA.

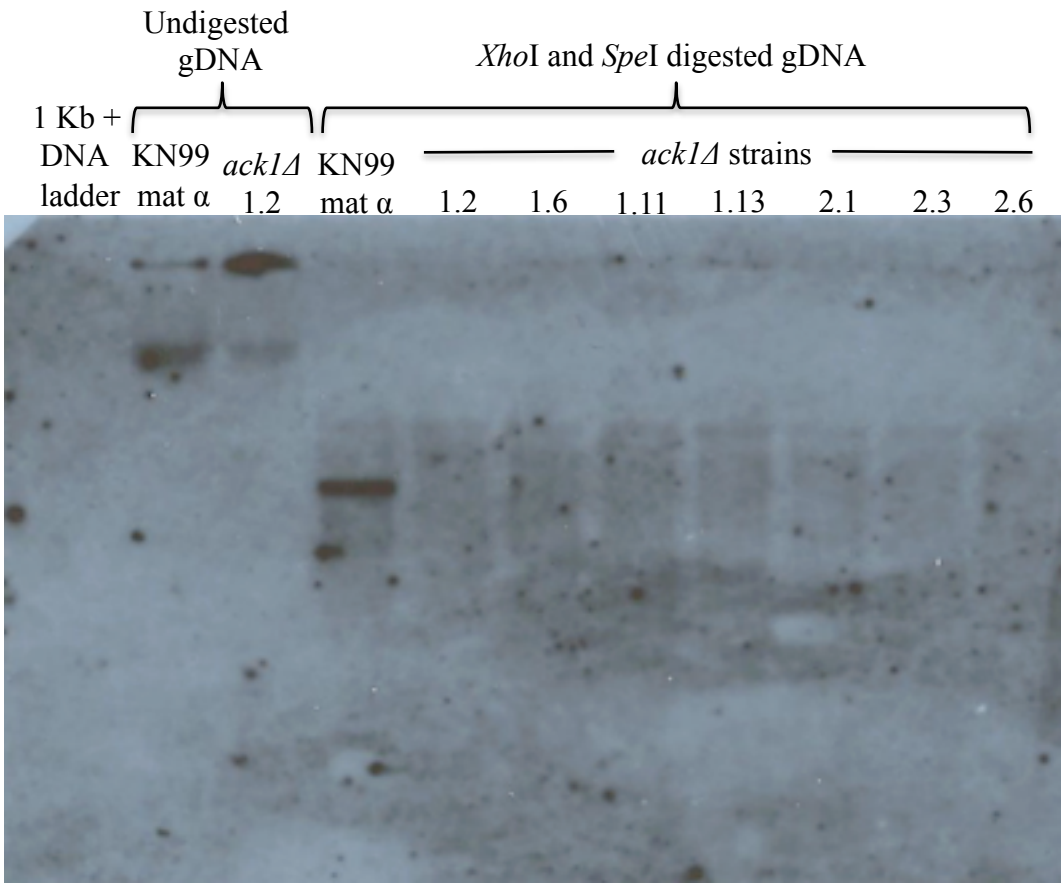

Figure 6: *ACK1* Southern Blot. Developed autoradiography film of the Southern blot using the *ACK1* probe.

Overlay of the autoradiography film and the gel image of digested gDNA of the *ACK1* probe Southern blot (Figure 7) allows size determination of the DNA fragments to which the *ACK1* probes hybridized. The blot overlay demonstrates that the single distinct band noted in the digested WT sample is located at approximately across from the 5 Kb ladder band. This finding corresponds to the expected fragment size to which we expected the *ACK1* probe to hybridize (5,053 bp).

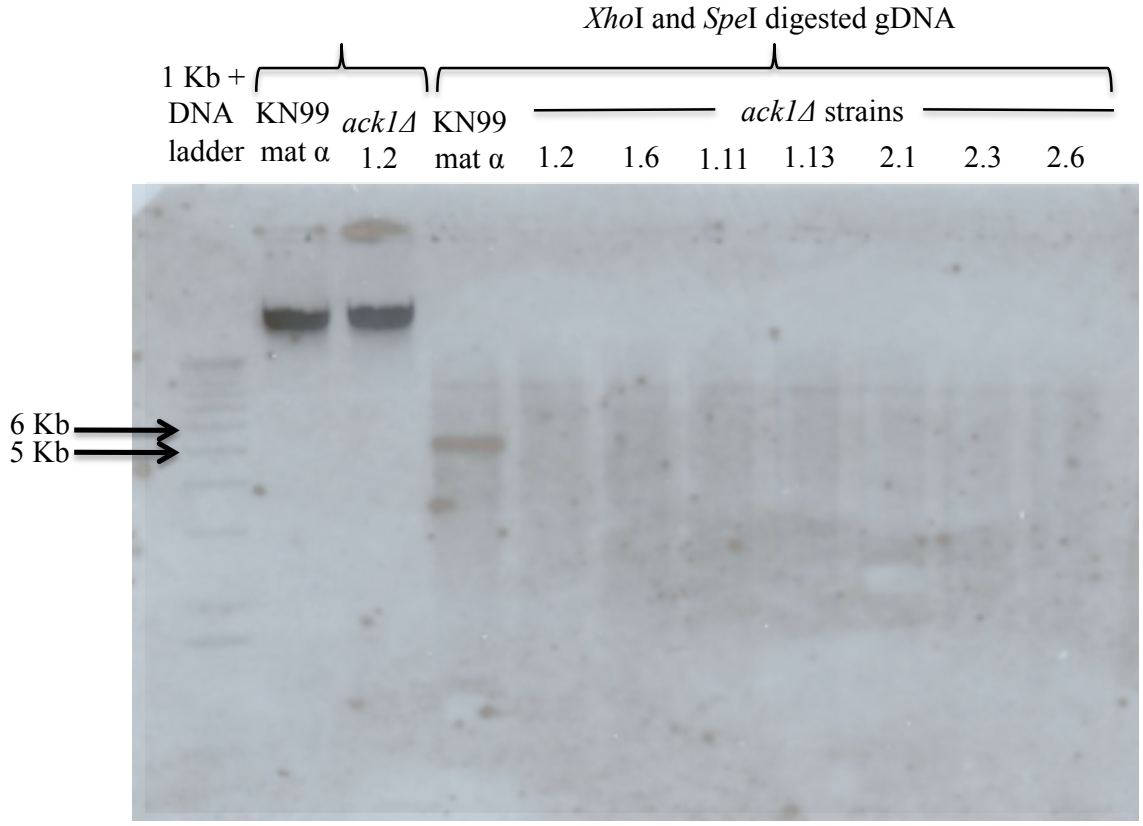

Figure 7: *ACK1* Southern Blot Overlay. Overlay of the *ACK1* probe film scan and the gel electrophoresis photograph.

The autoradiography film from the NEO^R probe blot exposure (Figure 8) demonstrates two dark bands near the top of the gel in lanes 1 and 2. A considerable amount of shadowing is noted running down each of the lanes containing digested gDNA. There are, however, areas of intense banding in two locations. There is a distinct intense band present higher up the blot present in the digested *ack1Δ* strain samples (lanes 5 through 11) but absent in the digested WT sample. There is also an intense distinct band noted further down the gel that is present in all of the digested gDNA

samples. The larger intense band that is present in the digested *ack1Δ* samples and not present in the digested WT sample is what we would expect to see with hybridization of the NEO^R probe. The smaller intense band that is present in all of the samples likely represents nonspecific binding of the probe because it is present in all of the samples. The smearing down the lanes also likely represents nonspecific binding of the NEO^R probe as well.

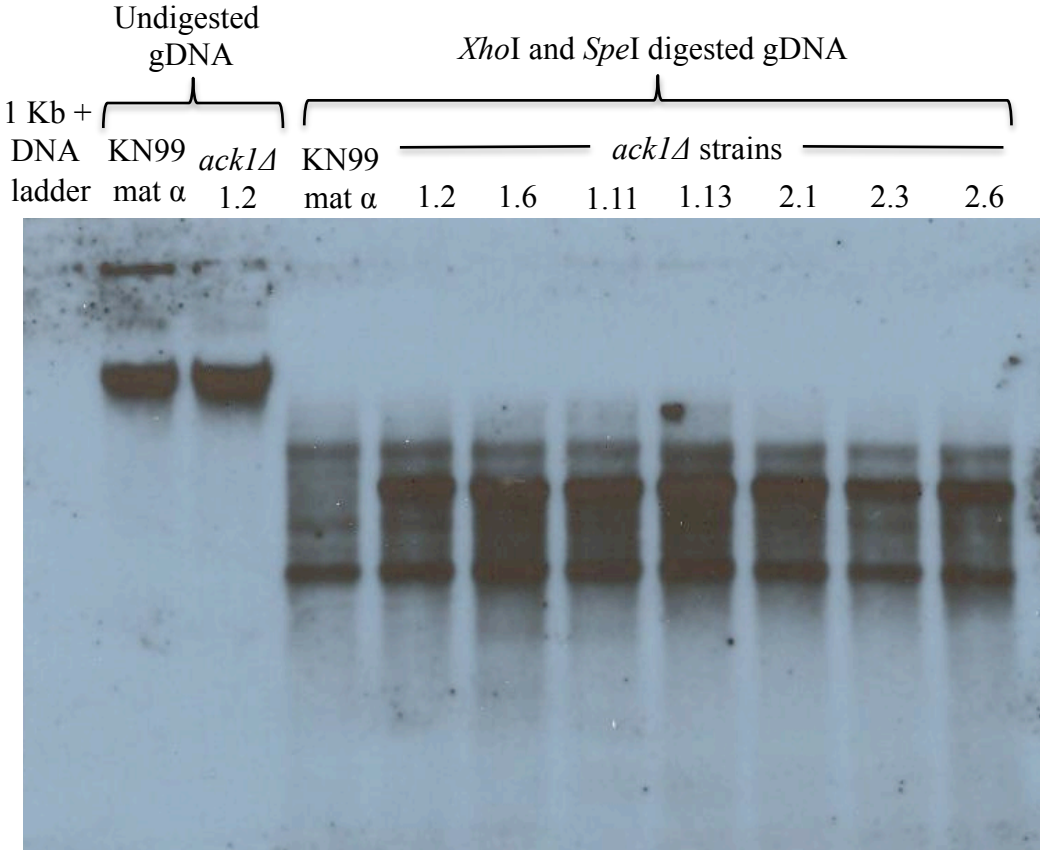

Figure 8: *NEO^R* Southern Blot. Developed autoradiography film of the Southern blot using the NEO^R probe.

The overlay of the autoradiography film and the gel image of digested gDNA (Figure 9) allows for size reference of the DNA fragments to which the *NEO*^{R} probes hybridized. The blot overlay demonstrates that the large intense banding higher up the blot demonstrates hybridization of the probe to a DNA fragment measuring approximately 6 Kb in size. This size corresponds to the expected size of DNA that we would expect the *NEO*^{R} probe to bind (6,073 bp). Notably, this intense band is not seen in the digested WT sample further demonstrating the absence of *NEO*^{R} in the WT strain. The smaller distinct intense band further down the blot in all the samples of digested gDNA likely represents strong nonspecific binding of the probe.

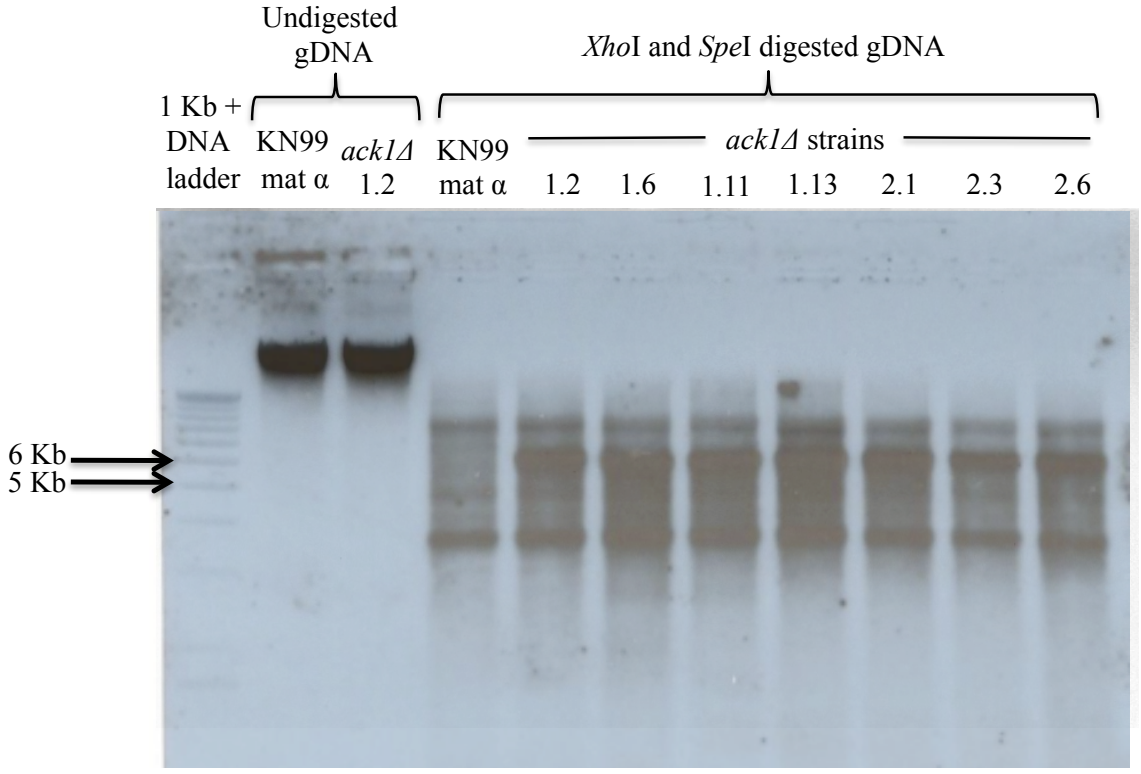

Figure 9: *NEO*^{R} Southern blot overlay. Overlay of the *NEO*^{R} probe film scan and the gel electrophoresis photograph.

The results of the Southern Blot demonstrate that the DNA sequence used in the *ACK1* probe is absent from the *ack1Δ* strains, and that they possess the NEO^R sequence used for the NEO^R probe.

Based upon the results of the cDNA analysis and Southern blot, in addition to the preliminary PCR that was performed when the strains were made, show that the *ack1Δ* construct strain integrated in to the correct location within the genome resulting in an absence of *ACK1* mRNA and subsequently Ack1p in the gene deletion strains.

Phenotype Characterization Studies

Carbon Source Utilization:

With the confirmation of a clean, single integration of NEO^R and removal of *ACK1*, as well as the absence of mRNA coding for *ACK1* in the gene deletion strains, the pursuit a unique phenotype in the *ack1Δ* strains was commenced. The first series of phenotype characterization experiments performed tested the *ack1Δ* strains' ability to utilize different sources of carbon at different concentrations. This was tested because bacteria utilize this acetate assimilation pathway as a way of handling excess Acetyl-CoA in high glucose environments. The experiments testing the *ack1Δ* strains' ability to utilize various carbon sources yielded similar growth rates and patterns between the WT and a variety of *ack1Δ* strains (Figure 10) on all of the carbon sources tested (Figures 11 - 18). The size of individual colonies, or lack thereof, was uniform amongst the strains. Additionally, growth on the 2% carbon places was noticeably better than those on the 0.2% carbon media. From these results it does not appear that absence of acetate kinase negatively or positively affects the utilization of the carbon sources tested.

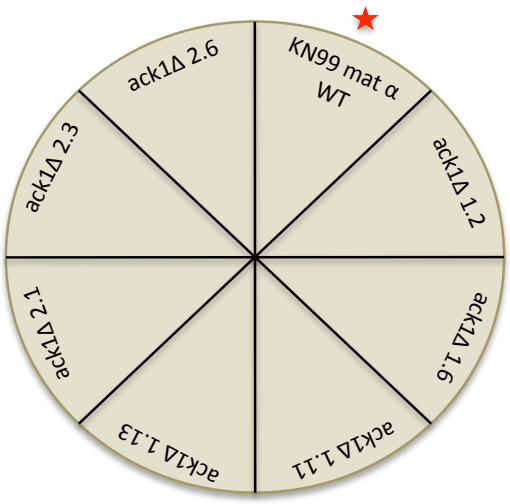

Figure 10: Strain Orientation for Phenotype Characterization. Diagram showing the strain identify on phenotype characterization plates. WT is denoted by star.

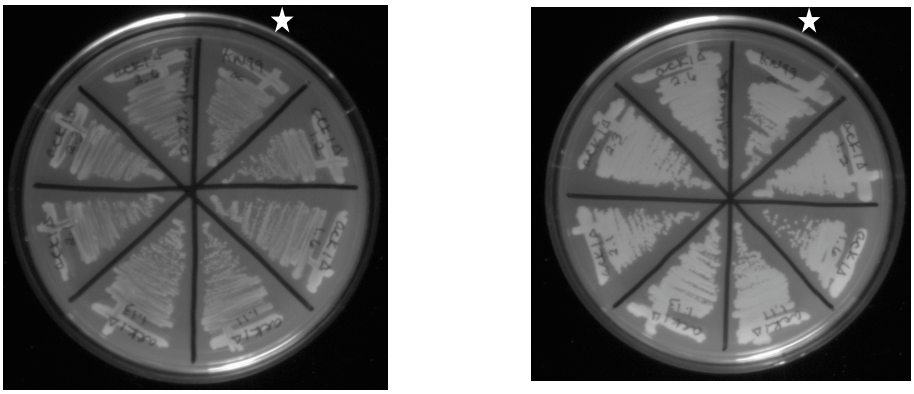

Figure 11: Growth on YNB + Glucose. Growth of KN99 mat α and *ack1Δ* strains 1.2, 1.6, 1.11, 1.13, 2.1, 2.3, and 2.6 on YNB (without amino acids) and 0.2% glucose (left) and 2% glucose (right).

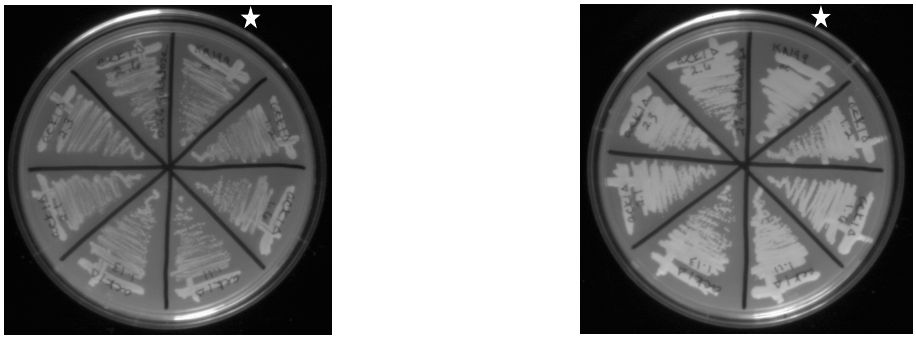

Figure 12: Growth on YNB + Galactose. Growth of KN99 mat α and *ack1Δ* strains 1.2, 1.6, 1.11, 1.13, 2.1, 2.3, and 2.6 on YNB (without amino acids) and 0.2% galactose (left) and 2% galactose (right).

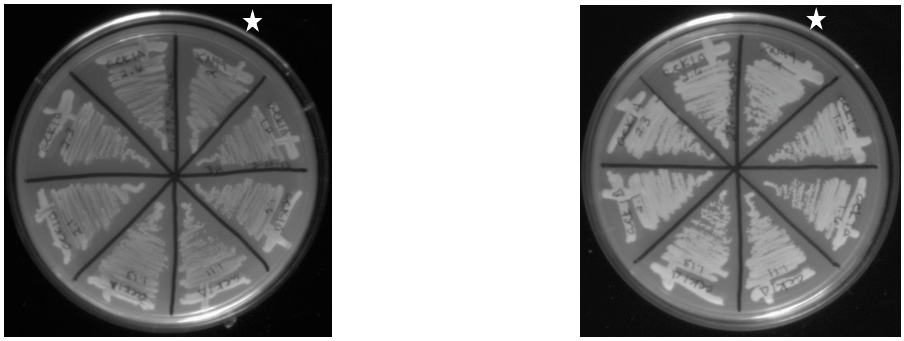

Figure 13: Growth on YNB + Sucrose. Growth of KN99 mat α and *ack1Δ* strains 1.2, 1.6, 1.11, 1.13, 2.1, 2.3, and 2.6 on YNB (without amino acids) and 0.2% sucrose (left) and 2% sucrose (right).

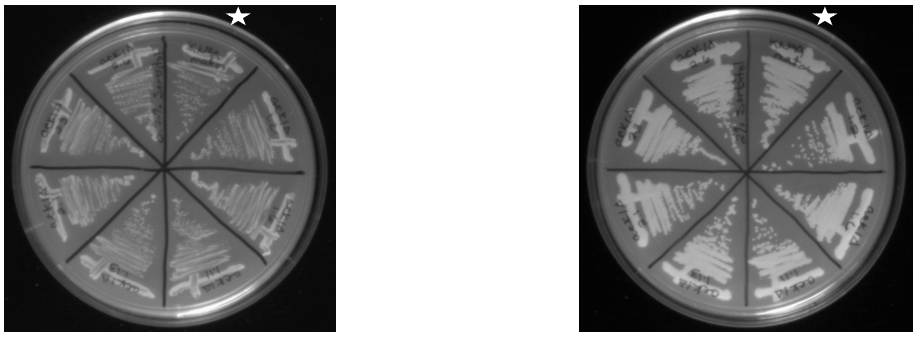

Figure 14: Growth on YNB + Sorbitol. Growth of KN99 mat α and *ack1Δ* strains 1.2, 1.6, 1.11, 1.13, 2.1, 2.3, and 2.6 on YNB (without amino acids) and 0.2% sorbitol (left) and 2% sorbitol (right).

Figure 15: Growth on YNB + Ethanol. Growth of KN99 mat α and *ack1Δ* strains 1.2, 1.6, 1.11, 1.13, 2.1, 2.3, and 2.6 on YNB (without amino acids) and 0.2% ethanol (left) and 2% ethanol (right).

Figure 16: Growth on YNB + Glycerol. Growth of KN99 mat α and *ack1Δ* strains 1.2, 1.6, 1.11, 1.13, 2.1, 2.3, and 2.6 on YNB (without amino acids) and 0.2% glycerol (left) and 2% glycerol (right).

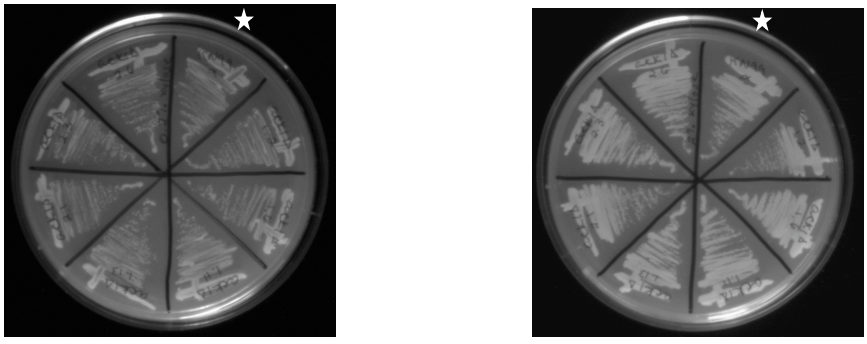

Figure 17: Growth on YNB + Xylose. Growth of KN99 mat α and *ack1Δ* strains 1.2, 1.6, 1.11, 1.13, 2.1, 2.3, and 2.6 on YNB (without amino acids) and 0.2% xylose (left) and 2% xylose (right).

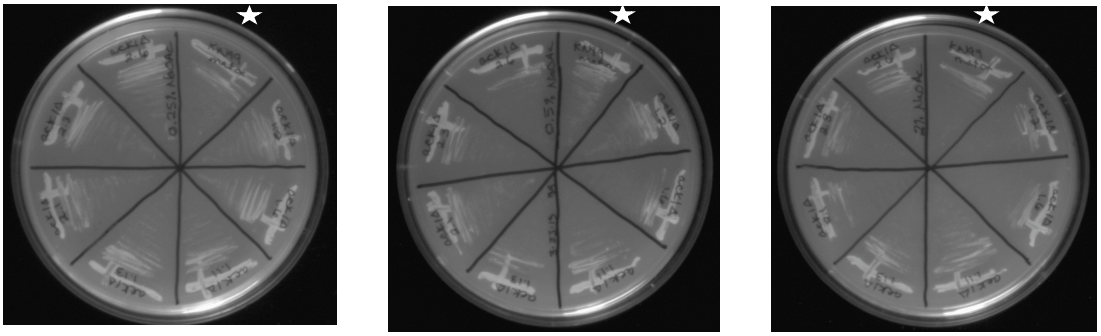

Figure 18: Growth on YNB + Sodium Acetate. Growth of KN99 mat α and *ack1Δ* strains 1.2, 1.6, 1.11, 1.13, 2.1, 2.3, and 2.6 on YNB (without amino acids) and 0.25% sodium acetate (left), 0.5% sodium acetate (middle), and 2% sodium acetate (right).

Temperature Sensitivity:

The *ack1Δ* strains were tested for temperature sensitivity as tolerance to the relatively warm temperature inside the human body (37˚C) is considered an important virulence factor. As demonstrated in Figure 19, all of the *ack1Δ* strains grew equally well as the WT strain at room temperature (~25˚C), 30˚C, 37˚C, and 40˚C. It is noted that growth is slightly less robust at RT, and the yeast begin to demonstrate growth inhibition at 40˚C. Based on these results, the absence of *ACK1* does not appear to demonstrate an alternate phenotype when subjected to the temperatures tested.

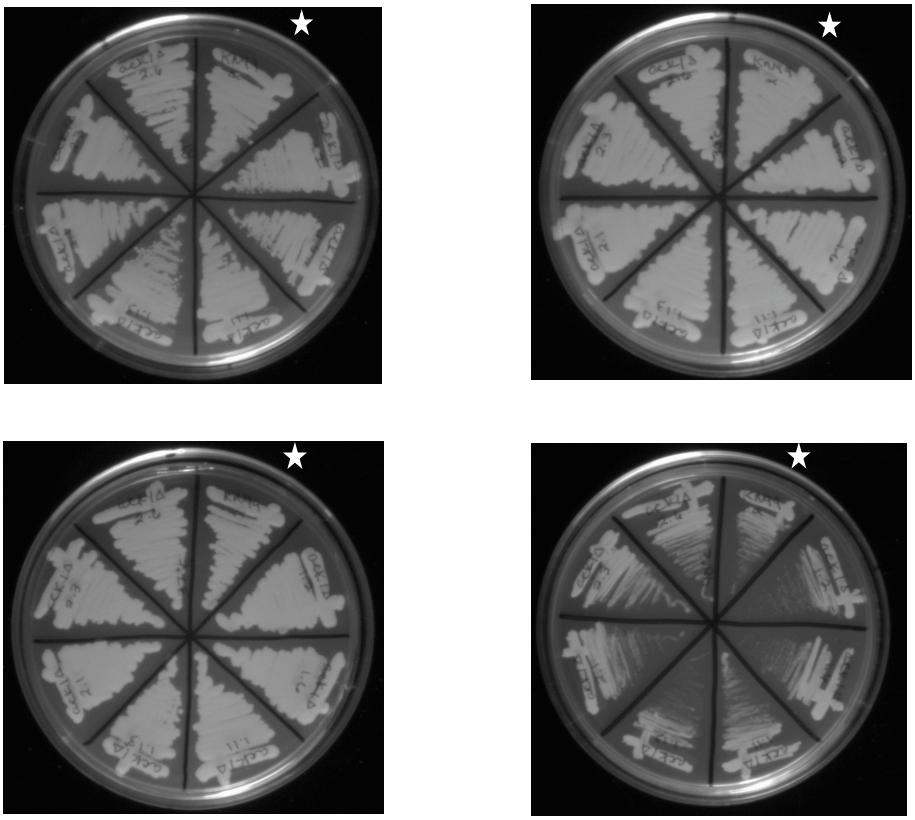

Figure 19: Temperature Tolerance on YPD. Growth of KN99 mat α and *ack1Δ* strains 1.2, 1.6, 1.11, 1.13, 2.1, 2.3, and 2.6 at RT (top left); 30˚C (top right); 37˚C (bottom left) 40˚C (bottom right).

Melanization:

Another important virulence factor of *C. neoformans* is its ability to produce melanin is another important virulence factor as it is believed to help protect the yeast from exposure to UV light and oxidative agents encountered in its environment or produced by phagocytic cells during an immune response to the pathogen (Casadevall and Perfect 1998). The results of the melanization experiment (Figure 20) demonstrate brown pigmentation of the samples indicative of melanin. The color of each colony appears to be the same shade of brown. The outcome of this experiment suggests that

melanization, considered a virulence factor in *C. neoformans*, is not affected by the deletion of *ACK1*.

Figure 20: Melanization. Growth KN99 mat α and *ack1Δ* strains 1.2, 1.6, 1.11, 1.13, 2.1, 2.3, and 2.6 on niger seed agar medium.

Nitrosative Stress:

Another phenotype associated with *C. neoformans'* pathogenicity is its ability to deal with the exposure to reactive nitrogen species such as nitric oxide that is experienced by pathogens following phagocytosis during the host immune response (Casadevall and Perfect 1998). The samples streaked onto the 0.75 mM sodium nitrite ($NaNO_2$) medium in Figure 21 all appear tolerate this stressor equally well. Again, there is no obvious difference in phenotype upon exposure to this nitrosative stress between the WT and the *ack1Δ* strains.

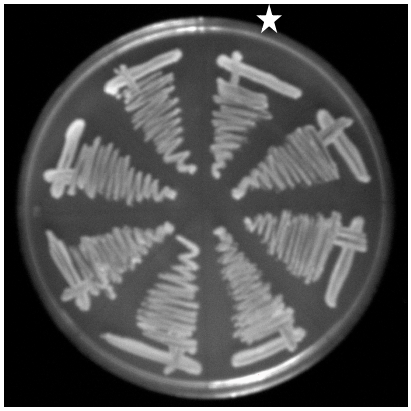

Figure 21: Growth Under Nitrosative Stress. Growth of KN99 mat α and *ack1Δ* strains 1.2, 1.6, 1.11, 1.13, 2.1, 2.3, and 2.6 on YNB (without amino acids) and 0.75 mM sodium nitrite.

Hypoxia-Mimicking Conditions:

The strains' ability to deal with hypoxic conditions is another characteristic of *C. neoformans* that enables it to cause systemic disease. In the absence of a functioning hypoxic chamber, hypoxic conditions were mimicked using $CoCl_2$. $CoCl_2$ mimics hypoxia by stabilizing a hypoxia-induced transcription factor (HIF1α) that, in the presence of oxygen is usually degraded (Ingavale et. al 2008). At 0.25 mM $CoCl_2$, the yeast were able to grow, however growth was significantly hindered at twice that concentration, and at 1 mM $CoCl_2$ growth was almost completely inhibited in all strains (Figure 22). Results of this experiment demonstrate that the phenotypic responses of all of the strains in response to the variable concentrations of $CoCl_2$ were consistent suggesting that Ack1p does not play a significant role in the yeast's ability to deal with a simulated hypoxic environment.

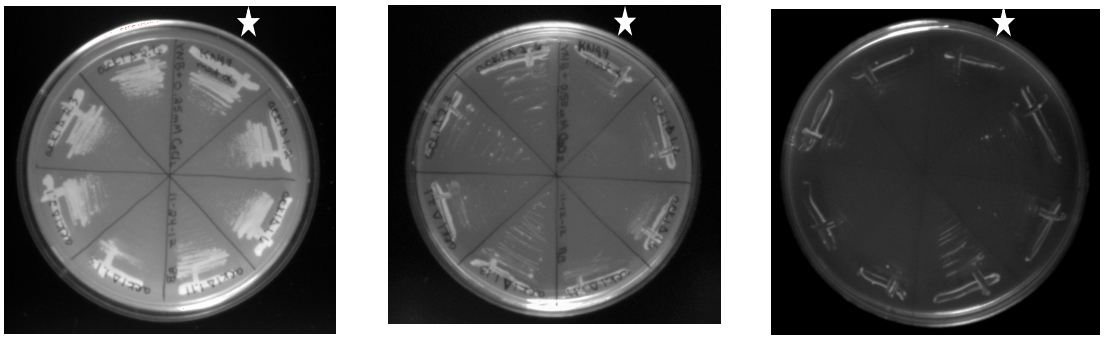

Figure 22: Growth Under Simulated Hypoxia. Growth of KN99 mat α and *ack1Δ* strains 1.2, 1.6, 1.11, 1.13, 2.1, 2.3, and 2.6 on YNB (without amino acids) and 0.25 mM $CoCl_2$ (left), 0.53 mM $CoCl_2$ (center), and 0.7 mM $CoCl_2$ (right).

pH:

The growth studies on media with variably adjusted pH demonstrated no difference in growth between the *ack1Δ* strains and the WT strains (Figure 23). Since *C. neoformans* is an environmental microorganism, it comes in contact with a variety of conditions to which it must be able to survive; however, it prefers more acidic environments such as bird, particularly pigeon, feces (Casadevall and Perfect 1998). In this experiment, all the strains grew similarly on each of the plates, with growth being slightly inhibited on the pH 11 medium. As a result, no difference in phenotype was identified in this experiment.

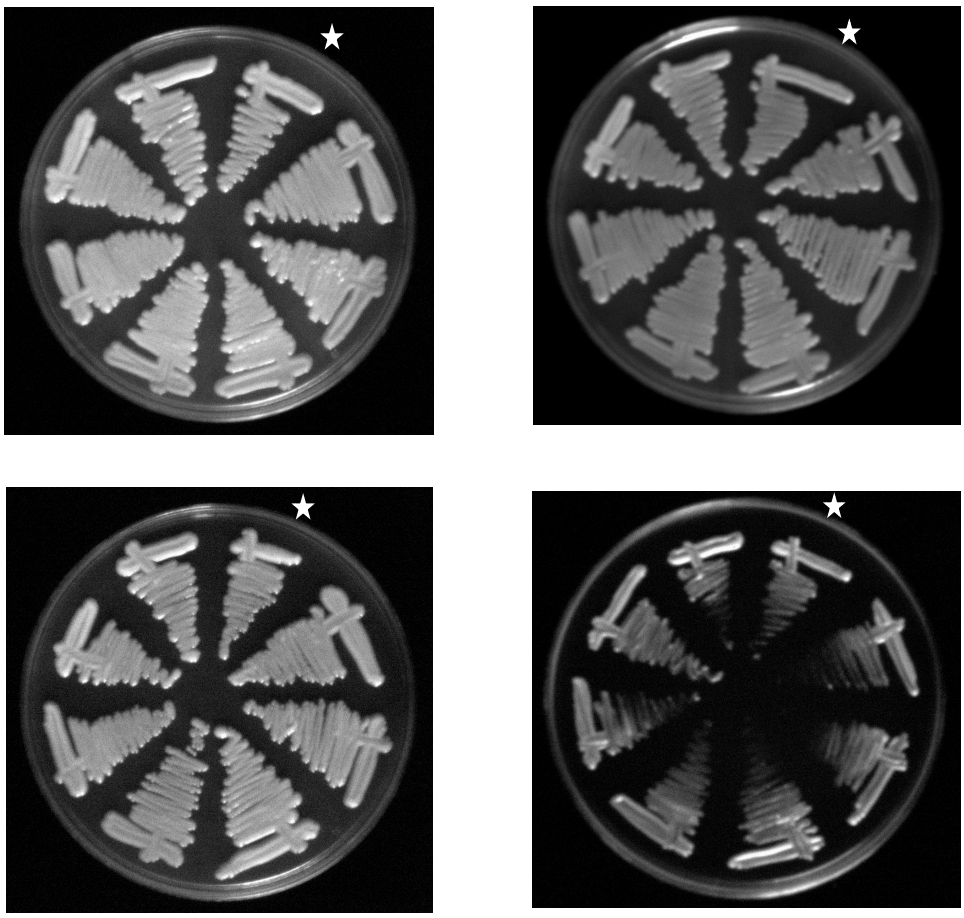

Figure 23: Effect of pH on Growth. Growth of KN99 mat α and *ack1Δ* strains 1.2, 1.6, 1.11, 1.13, 2.1, 2.3, and 2.6 on YPD (without amino acids) at pH 5 (top left), pH 7 (top right), pH 9 (bottom left), pH 11 (bottom right).

Filamentation During Sexual Reproduction:

While *C. neoformans* primarily reproduces asexually via budding, interaction between the two mating types, mat a and mat α, result in the production of filaments and basidiospores. While cryptococcosis most commonly manifests itself in the lungs, it is not definitively known if inhalation of basidiospores or desiccated yeast cells are the culprit (Casadevall and Perfect 1998). The ability of the *ack1Δ* strains to produce filaments indicative of sexual reproduction demonstrated no phenotypic difference

(Figure 24). Filamentation observed in the WT strain as well as the *ack1Δ* strains were present in similar abundance. Interestingly, upon completion of this experiment it was noted that the *ack1Δ* strains, originally believed to be of the mating type-α, were instead of the mat-a mating type. This was discovered because the *ack1Δ* strains only mated and produced filaments with the WT mat-α strain. This was discussed and is believed that the phenotypes explored in this study would not be affected by mating type.

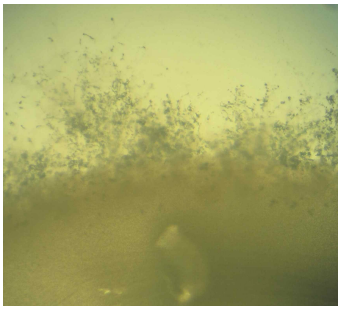

KN99 mat α X KN99 mat a

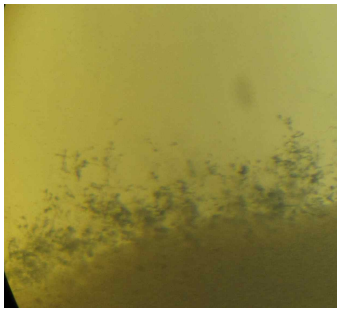

KN99 mat α X *ack1Δ* 1.2

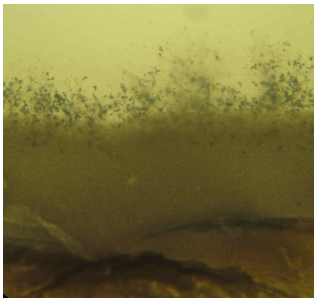

KN99 mat α X *ack1Δ* 1.6

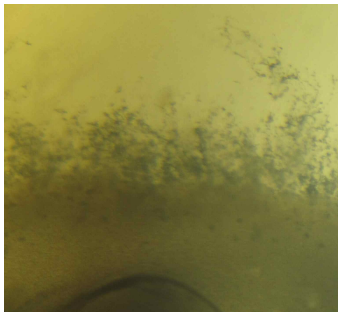

KN99 mat α X *ack1Δ* 1.11

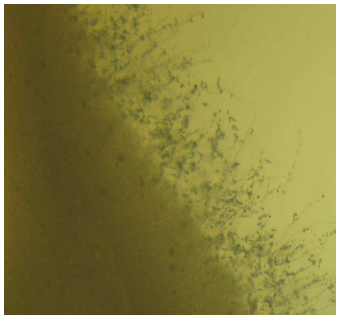

KN99 mat α X *ack1Δ* 1.13

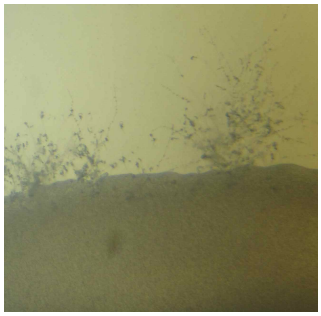

KN99 mat α X *ack1Δ* 2.1

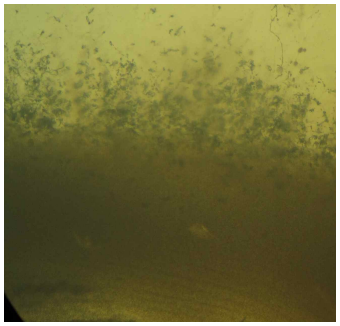

KN99 mat α X *ack1Δ* 2.3

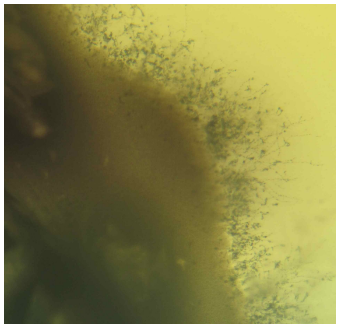

KN99 mat α X *ack1Δ* 2.6

Figure 24: Filamentation During Sexual Reproduction. Hyphal filamentation from mating of KN99 mat α and *ack1Δ* strains 1.2, 1.6, 1.11, 1.13, 2.1, 2.3, and 2.6 on Murashige-Skoog medium.

Oxidative Stress:

The response to oxidative stress experienced upon exposure to varying concentrations of H_2O_2 was tested using *ack1Δ* strains and the WT strain. Similar to nitrosative stress, pathogenic microorganisms are exposed to reactive oxygen species by the phagocytic cells of the host's immune system (Casadevall and Perfect 1998). All of the strains except *ack1Δ* 1.13 grew on the medium containing 0.25 mM H_2O_2 and growth was absent from all strains at 0.5 mM and 1 mM H_2O_2 (Figure 25). Although *ack1Δ* 1.13 did show different phenotypes than the WT, it appears unlikely that the difference can be attributed to the *ACK1* deletion since no other *ack1Δ* strain exhibits this unique phenotype. It is likely that this phenotype is the result of a second gene mutation, and resolving this interesting result would make an interesting classic forward genetic study. As for the other *ack1Δ* strains, it appears that no phenotypic difference was found in the strains' ability to deal with the oxidative environment to which they were subjected.

Figure 25: Oxidative Stress Phenotypes. Growth of KN99 mat α and *ack1Δ* strains 1.2, 1.6, 1.11, 1.13, 2.1, 2.3, and 2.6 on YNB (without amino acids) and 0.25 mM H_2O_2 (left), 0.5 mM H_2O_2 (center) and 1 mM H_2O_2 (right).

Cluster Growth Phenotype:

Several attempts at performing a growth curve on the cells were made however clustering or "clumping" of the cells inhibited accurate cell counts. Initially, it was thought that only the *ack1Δ* strains were exhibiting this phenotype so attention was directed to definitively determining if this phenomenon was unique to the mutant strains. Observations of the WT and several of the deletion strains grown in YPD (50 g/L) and in minimal media demonstrated that none of the strains grown in YPD (50 g/L) exhibited the clustering phenotype, and all of the strains grown in minimal media demonstrated this effect (Figures 26 and 27). It is believed that the yeasts' reaction to the minimal medium is resulting in this phenomenon rather than the result of the gene deletion.

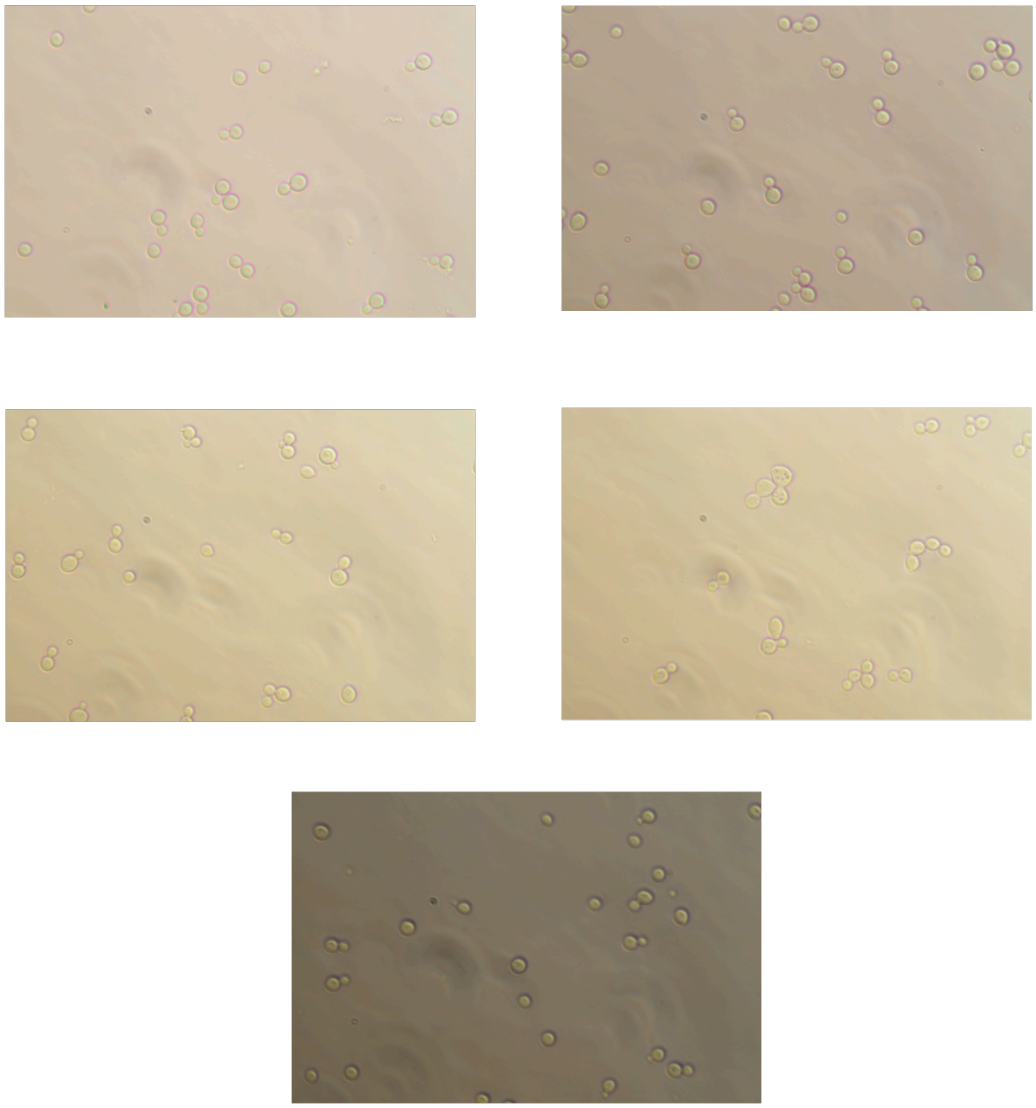

Figure 26: Clustering Phenotype in YPD. Growth of KN99 mat α (top left); *ack1Δ 1.2* (top right); *ack1Δ 1.11* (middle left); a*ck1Δ 1.13* (middle right); *ack1Δ 2.3* (bottom) in YPD at 30˚C.

Figure 27: Clustering Phenotype in Minimal Medium. Growth of KN99 mat α (top left); *ack1Δ 1.2* (top right); *ack1Δ 1.11* (middle left); a*ck1Δ 1.13* (middle right); *ack1Δ 2.3* (bottom) in YPD at 30˚C.

Polysaccharide Capsule Formation:

Perhaps one of the most important virulence factors and one of the most striking characteristics *C. neoformans* possesses is the ability to synthesize a polysaccharide capsule. It is believed that this capsule serves numerous functions including offering protection from environmental conditions and hindering phagocytosis (Casadevall and Perfect 1998). According to the observations made following incubation in the capsule-inducing medium, there is a pronounced white halo surrounding the WT and the *ack1Δ* strain cells following staining with India ink, demonstrating their ability to synthesis a capsule (Figure 28). Notably, however, *ack1Δ* 1.13 appears to make a more robust capsule than is seen in all of the other strains tested. With the exception of *ack1Δ* 1.13, the capsules visually appear similar to those demonstrated by the WT. The capsules vary considerably in size within each sample, and the cells appear to be more clustered, similar to those encountered in the cluster growth phenotype experiment. This is possibly due to the nutrient poor medium in which these cells were grown. According to these results, it does not appear that *ACK1* visibly affect the synthesis of the polysaccharide capsule.

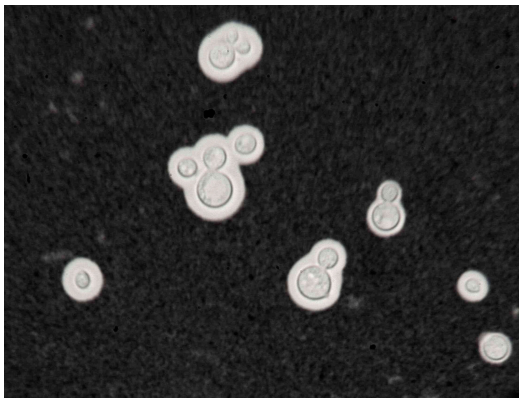

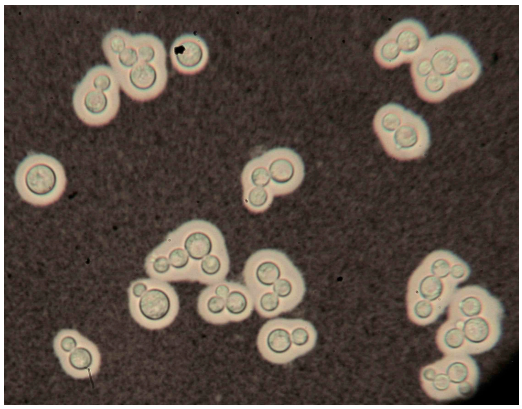

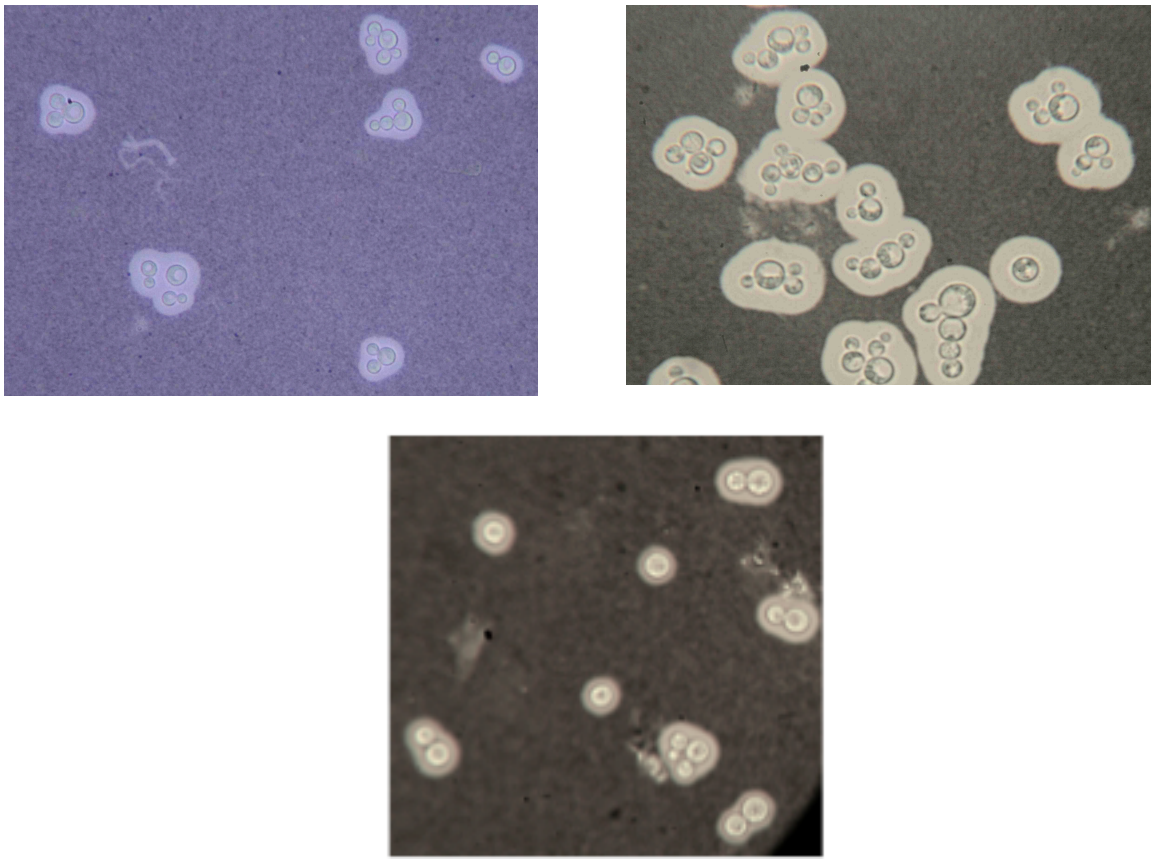

Figure 28: Polysaccharide Capsule Formation. Capsule formation of KN99 mat α (top left – previous page), a*ck1Δ 1.4* (top right - previous page), *ack1Δ 1.6* (middle left), and *ack1Δ 2.4* (bottom) in capsule inducing medium.

Cell Wall Integrity:

In addition to secreting a polysaccharide capsule, *C. neoformans* possesses a cell wall that provides structure and protection for the cell. The cell wall integrity of the *ack1Δ* strains was tested with SDS and Congo Red stain (Figure 29). The mutant strains

tolerated the amphiphilic property of the SDS. Likewise, the WT and *ack1Δ* strains demonstrated no phenotypic difference when exposed to Congo red stain.

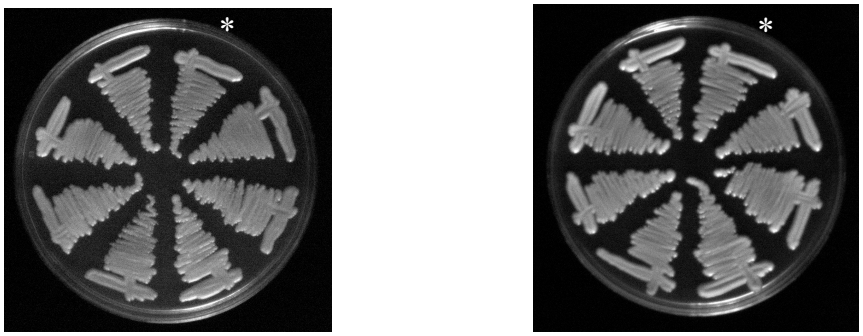

Figure 29: Cell Wall Integrity. Growth of KN99 mat α and *ack1Δ* strains 1.2, 1.6, 1.11, 1.13, 2.1, 2.3, and 2.6 on YNB (without amino acids) + 0.01% SDS (left) and on YNB + 0.5% Congo Red (right).

ACK1 Complementation Construct for Electroporation

Construction of a plasmid that could be utilized to expression *ACK1* in the gene deletion strains following discovery on a unique phenotype was successful. The hope is that any deviation of phenotype expressed by the *ack1Δ* strains would be reverted back to the WT phenotype upon expression of *ACK1* via this plasmid-based complementation construct.

The first part of this project involved PCR amplification of *ACK1* using primers with sequences approximately 1 Kb upstream and approximately 250 bp downstream of *ACK1*. *Spe*I restriction sites were added to the 5' end of the sense primer (BLO11) and to the 3' end of the antisense primer (BLO12). These *Spe*I sites were used for insert and vector ligation. The *ACK1* insert and the pHYG7-KB1 vector were both digested with

*Spe*I in preparation for the ligation reaction. The gel image of the digested and purified pHYG7-KB1 vector in lane 2 (Figure 30) demonstrates a single clean band located near the 5 Kb and 6 Kb bands of the DNA ladder. This corresponds to the expected length of the vector of 5,661 bp. The gel of the digested and purified *ACK1* insert demonstrates a single clean band located slightly above the 3 Kb band of the ladder, corresponding to the expected length of 3,041 bp. The bands of the vector and insert appear to be similar of intensity indicating a similarity in DNA concentration. Visualization of ligation components aids in the determination of volume used in the ligation reactions.

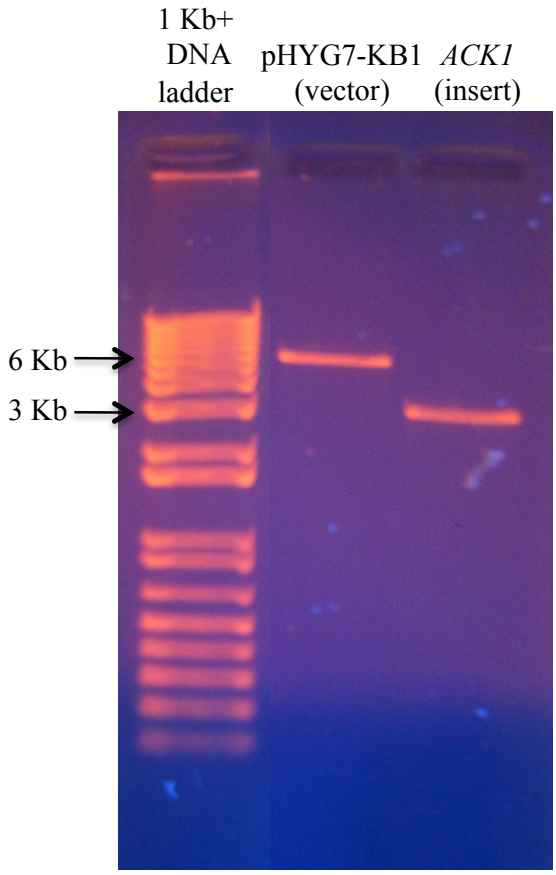

Figure 30: *ACK1* Complementation Construct Components. *Spe*I digested pHYG7-KB1 vector and *ACK1* insert used for constructing the *ACK1* complementation plasmid.

Bacterial transformation of the ligation reaction on LB + Amp plates yielded 48 colonies. Twenty-six colonies were present on the linearized vector plate and no colonies were noted on the control plate. The absence of colonies on the control plate indicates that the selectable marker ampicillin is working. The only colonies that arise on this medium should have taken in the plasmid that confers resistance to ampicillin. As noted in the results of the transformation, fewer *E. coli* cells are successfully transformed with linearized vectors.

Colony PCR was used to quickly identify transformants containing the *ACK1* complementation construct. Primers KIO21 and KIO22, consisting of *ACK1* sequences, were used to amplify a 516 bp segment of this gene. The gel image of the colony PCRs (Figure 31) performed on the first eight colonies from the transformation plate demonstrates bright, clean, single bands located just above the 500 bp band of the DNA ladder from colonies #2 and #7. This corresponds to the expected size of the PCR product. None of the other colonies demonstrated amplification.

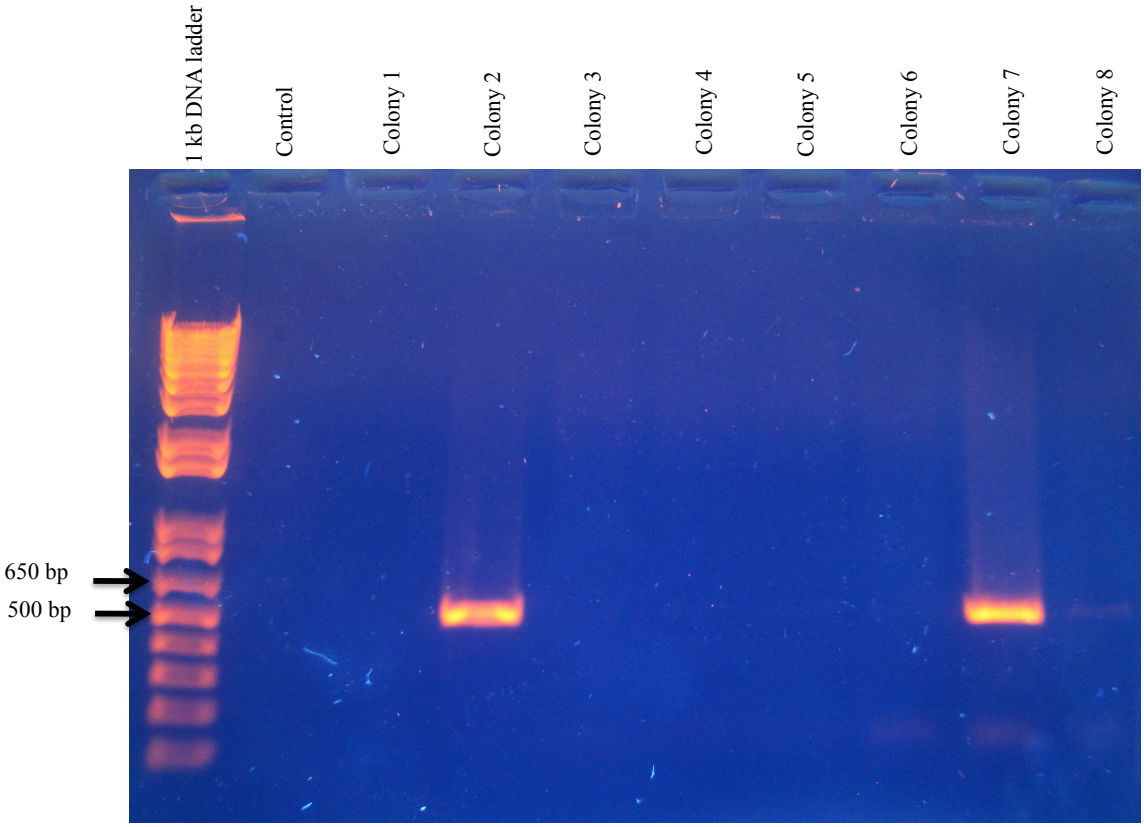

Figure 31: Colony PCRs from the *ACK1* Complementation Ligation. Colony PCRs of colonies #1 - #8 following transformation of *E. coli* with the *ACK1* complementation plasmid.

A *Xba*I restriction digest was performed to determine the orientation of the *ACK1* insert into the vector. This endonuclease was chosen because there are two *Xba*I restriction sites present in the construct, one located near one ligation site and the other present near one end of the construct. The *Xba*I restriction sites are situated close to one another with an antisense orientation of the insert. A *Xba*I restriction digest on an antisense oriented insert is expected to produce two fragments measuring 315 bp and 8,383 bp. However, because one fragment is so small, in order to allow adequate

separation of the larger fragments the gel could possibly demonstrate only a single band measuring approximately 8 Kb. Ligation of the *ACK1* insert in the sense orientation would situate the two *Xba*I restriction sites further apart. Following a *Xba*I restriction digest of a construct of this type, two fragments, one measuring 2,730 bp and the other measuring 5,968 bp would be anticipated.

The gel of the *Xba*I digests of gDNA from colonies #2 and #7 (Figure 32) demonstrates two different results from the two colonies. The digest of colony #2 gDNA demonstrates two bands, one located just below the 3Kb band of the ladder and the other located at approximately the 6 Kb band of the ladder. These products correspond to a sense orientation of the *ACK1* insert in the *ACK1* complementation construct. The digest of colony #7 gDNA demonstrates a single large band located at approximately between the 8 and 9 Kb bands of the ladder. This result corresponds to an antisense orientation of the *ACK1* insert in the *ACK1* complementation construct. So, by chance, both insert orientations were obtained from the two colonies tested.

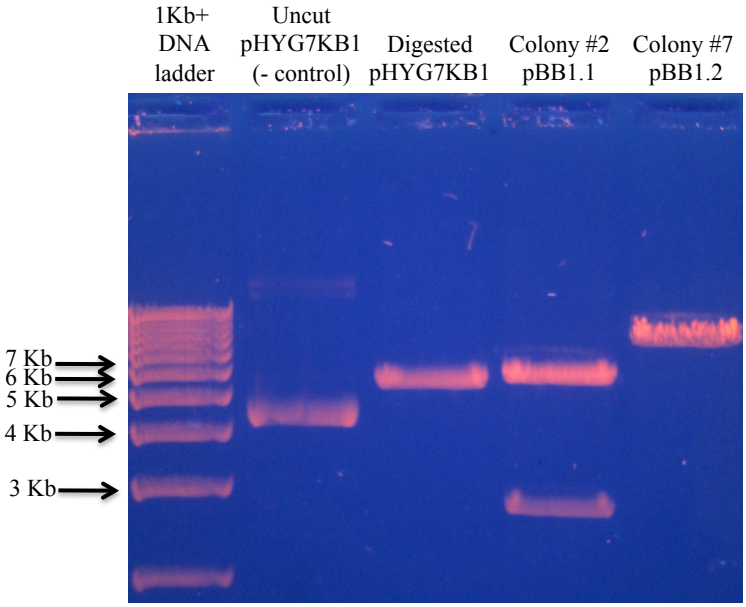

Figure 32: *Xba*I Digest for *ACK1* Insert Orientation. Gel electrophoresis of the uncut vector (pHYG7-KB1) and *Xba*I digested pHYG7-KB1, colony #2, and colony #7 for *ACK1* insert orientation determination within the *ACK1* complementation plasmid.

ACK1-mCherry Strain Development

The purpose of creating these *ACK1-mCherry* strains was to hopefully enable visualization of where AK is utilized within the cell. This is performed by inserting the sequence that codes for a small red fluorescent protein direction adjacent to the end of AK, removing the *ACK1* stop codon in the process. Not only with this allow for subcellular localization of AK, but it will also allow AK to be purified from cell lysate using anti-mCherry beads. Protein isolated from the cell could then be used for enzyme kinetic studies.

The initial approach to developing the *ACK1-mCherry* strain was to produce the construct using overlap PCR in which three fragments that comprise the construct each contain small overlapping sequences on the 5' and 3' ends of the adjacent fragments. Following many unsuccessful attempts, an alternative method was utilized. This approach involved the introduction of specific restriction sites or utilization of existing restriction sites at the 5' and 3' ends of adjacent components of the construct as well as the vector (pCR2.1 Topo) into which the construct is cloned. As demonstrated in Figure 33, a *Bam*HI site was introduced into the sense primer (KIO27) for the PCR of the first fragment that contains the *ACK1* promoter and *ACK1*. A single *Bam*HI site present in the vector was used to ligate the 5' end of the construct to the vector. Additionally, there is not a *Bam*HI site present in fragment 1 which allows digestion of the 5' end *Bam*HI site without cutting another site within the fragment. The antisense primer (KIO28) was designed to remove the *ACK1* stop codon and introduce a *Spe*I site on the 3' end. Like the *Bam*HI site, there is no other *Spe*I site in fragment 1 which allowed digestion of the 3' end *Spe*I site without disrupting the rest of the fragment.

The second fragment, consisting of *mCherry* and NEO^R, was prepared using primers KIO29 and KIO30 that introduced a *Spe*I site on the 5' end and a *Nde*I site on the 3' end. The *Spe*I site was specifically chosen to link fragments 1 and 2 due to the fact that it is a 6 base pair restriction site. This would allow the linking of *ACK1* with *mCherry* without causing a shift in the codon reading frame.

The third fragment consisting of the 3' untranslated region of *ACK1* was prepared using a sense primer (KIO31) that introduced an *Nde*I site on the 5' end to which the 3' end of the second fragment ligated. The antisense primer of fragment 3 (KIO32)

introduced a *Kpn*I site to the 3' end of the fragment. This end was ligated to the single *Kpn*I site present in the vector.

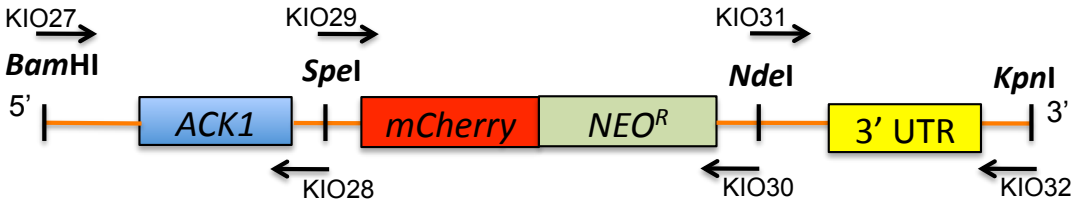

Figure 33: *ACK1-mCherry* Construct. Diagram of the *ACK1-mCherry* construct demonstrating the primers used to amplify each fragment and the restriction sites used to ligate the construct together.

Following amplification of the three fragments comprising the *ACK1-mCherry* construct, restriction digests using the appropriate endonucleases were performed on these fragments as well as the vector, pCR2.1 TOPO. These restriction digests were PCR purified and visualized via gel electrophoresis. As demonstrated in Figure 34, the sizes of each fragment and the vector correspond to the expected sizes of 2,748 bp for fragment #1, 3,200 bp for fragment #2, 1,012 bp for fragment #3, and 3,908 bp for the vector. Additionally, the gel was used to determine the relative concentrations of each component of the construct to help determine component volumes used in the ligation reactions. Fragments 1 and 3 appear very similar in concentration, fragment 2 appears to be of lowest concentration, and the vector appears to be the most concentrated of all the components.

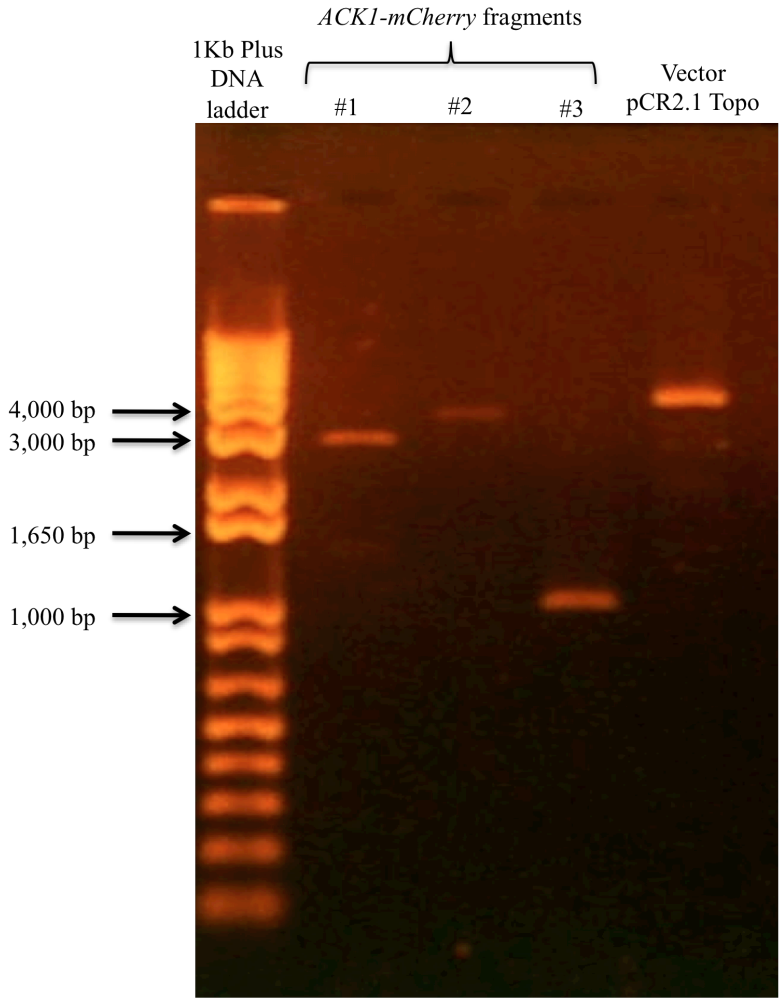

Figure 34: Digested and Purified *ACK1-mCherry* Construct Fragments. Gel electrophoresis of *Bam*HI and *Spe*I digested and purified fragment #1, *Spe*I and *Nde*I digested and purified fragment #2, *Nde*I and *Kpn*I digested and purified fragment #3, and *Bam*HI and *Kpn* digested and purified vector.

Following ligation and transformation of the ligation reaction into DH5α competent *E. coli* cells, colony PCRs using primers KIO21 and KIO22 were performed to rapidly determine the presence of *ACK1* within the transformants. Figure 35 demonstrates the gel image of a series of colony PCRs that were performed on the transformation colonies. A faint band is noted in numerous samples located just above

the 500 bp band of the marker. Colony #A8 demonstrates a single bright band at the same location. This fragment size corresponds to the expected fragment size of 516 bp resulting from the primers utilized and the presence of *ACK1*.

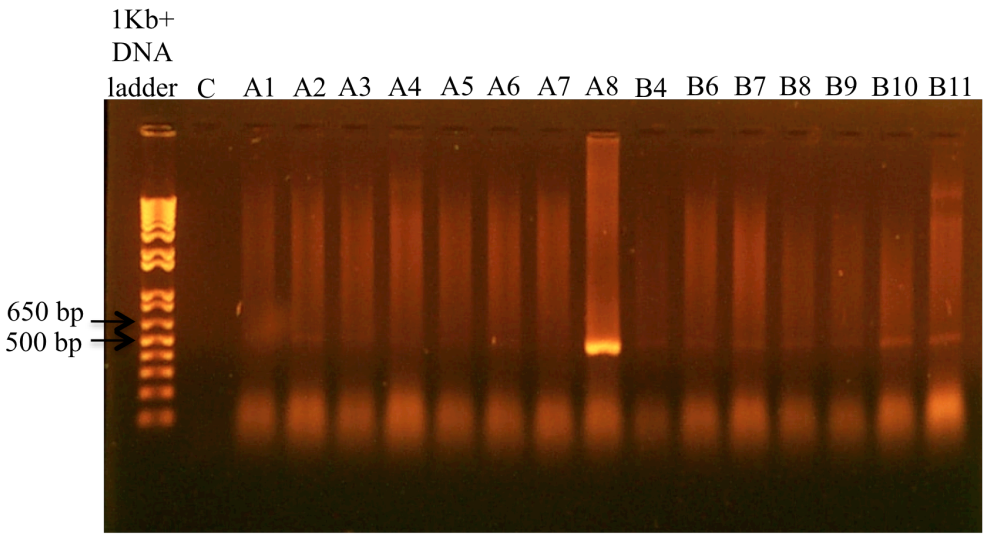

Figure 35: Colony PCR of *ACK1-mCherry* Transformants. Colony PCR products from colonies A1-A8 and B6-B11 following transformation of competent *E. coli* using the ligation reaction of the *ACK1-mCherry* construct.

To confirm the presence of the entire *ACK1-mCherry* construct, minipreps were performed on colony #A8, the colony that demonstrated the bright single band following colony PCR, as well as colonies #B6, #B7, #B10, and #B11, colonies that demonstrated a faint band at the expected location, and a *Xho*I restriction digest was performed on the plasmid DNA. The gel image of the products of the *Xho*I digest (Figure 36) demonstrates undigested A8 plasmid DNA (negative control) in lane 2, and two distinct bands are noted in the colony A8 sample, the larger of which is located around the 7 Kb band of the ladder and the smaller fragment located just above the 4 Kb marker of the ladder. A

single bright band located at around the 4 Kb marker is noted in the digest of colonies B6, B7, and B10, and a single bright band located between the 5 Kb and 6 Kb markers of the DNA ladder. The plasmid DNA from colony A8 is the only sample that demonstrates the expected fragment sizes of 4,011 bp and 6,774 bp resulting from a *Xho*I digest of the complete *ACK1-mCherry* construct plasmid (Figure 37).

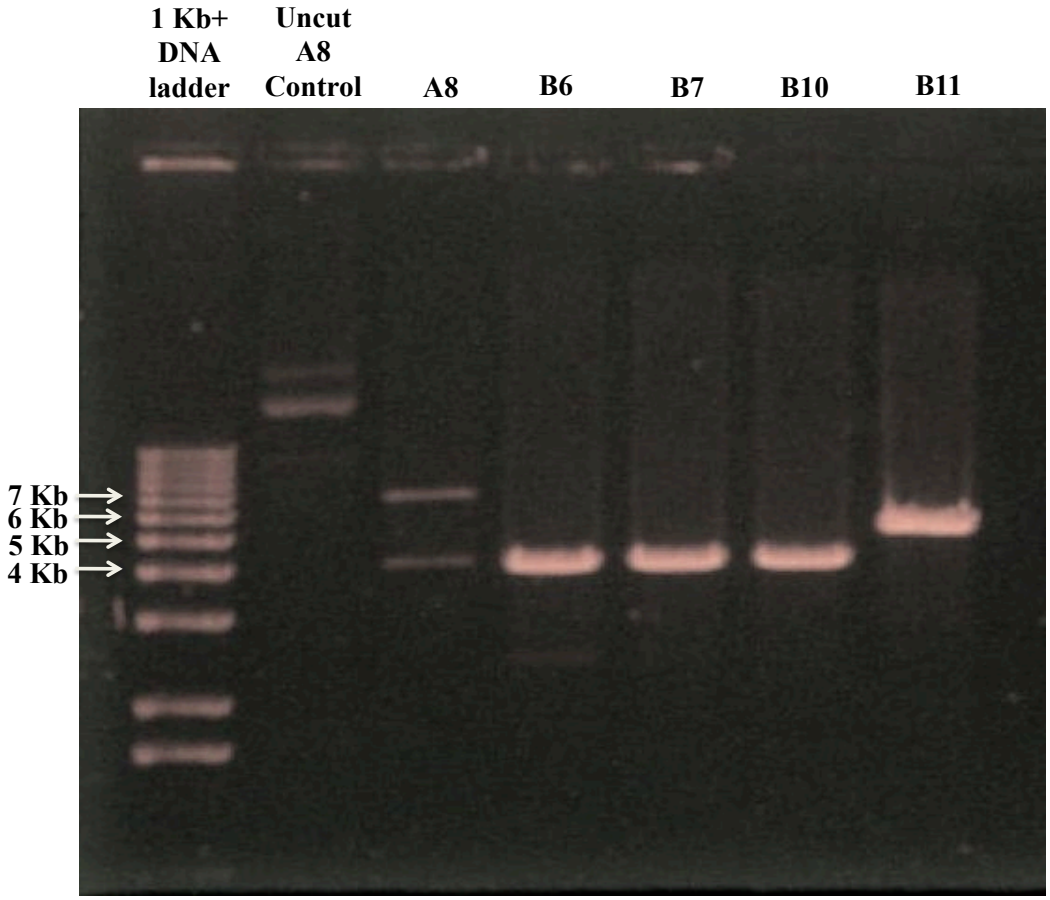

Figure 36: *Xho*I Restriction Digest of *ACK1-mCherry* Construct. *Xho*I restriction digest on minipreps from colonies A8, B6, B7, B10, and B11 for confirmation of complete *ACK1-mCherry* construct.

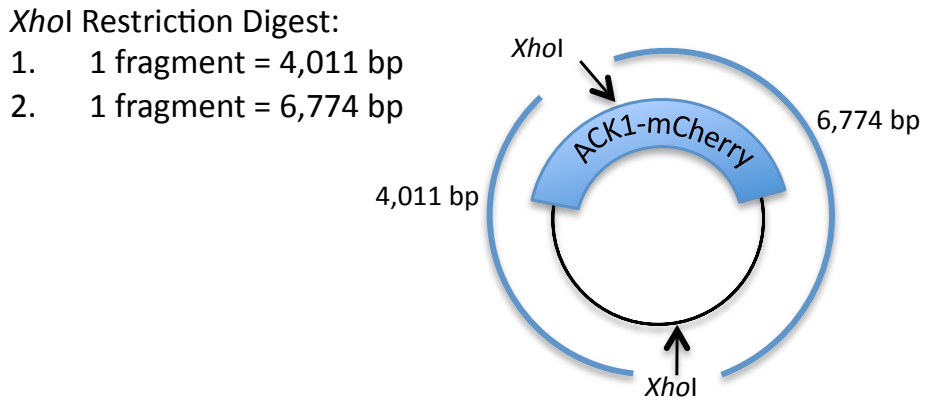

Figure 37: *Xho*I Restriction Sites Within the *ACK1-mCherry* Plasmid. Diagram demonstrating expected fragments expected from a *Xho*I restriction digest of the *ACK1-mCherry* plasmid.

Following *Xho*I digest confirmation of the plasmid, the entire *ACK1-mCherry* construct was PCR amplified and purified in preparation for biolistic transformation of KN99 mat α cells. The sense primer of the first fragment (KIO27) and the antisense primer of the third fragment (KIO32) were used to amplify the entire construct. Figure 38 demonstrates the products of four *ACK1-mCherry* construct PCRs each consisting of a single band of varying concentrations each located at around the 7 Kb band of the DNA ladder. This fragment size corresponds to the expected size of 6,900 bp. Each reaction contains the same components and only varies by annealing temperature. Good amplification is demonstrated with the annealing temperatures of 63˚C (sample #2), 63.5˚C (sample #3), and 64˚C (sample #4).

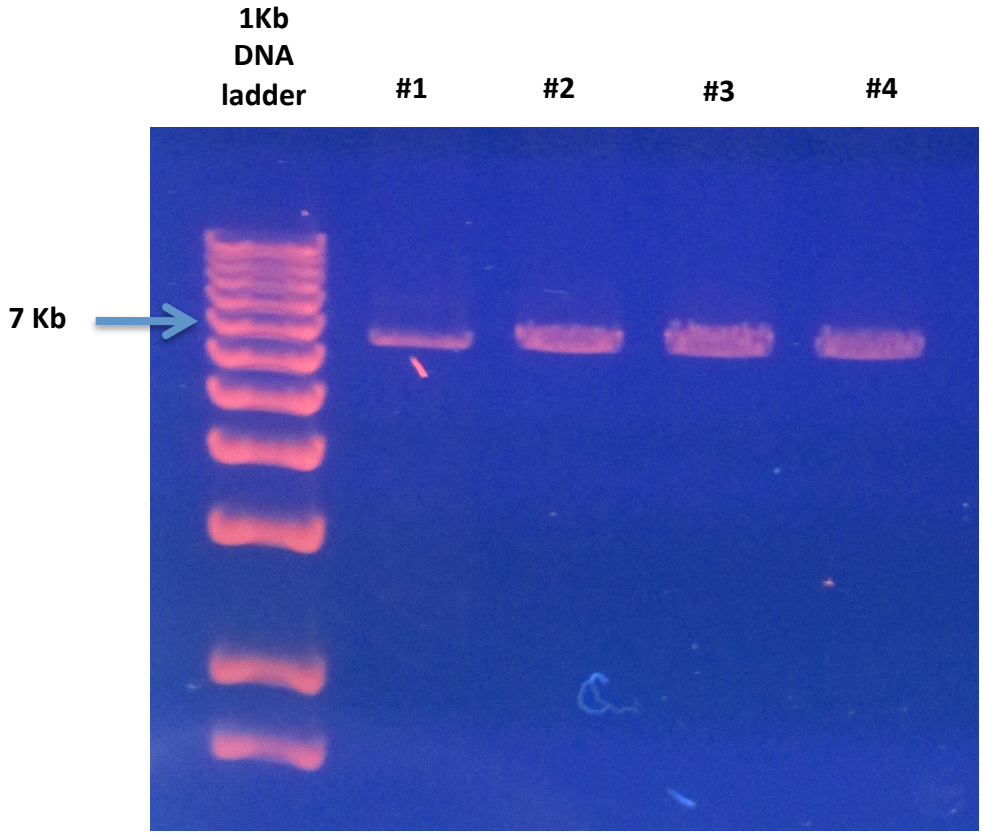

Figure 38: PCR of A*CK1-mCherry* Construct. The gel demonstrates amplification of the 6,900 bp *ACK1-mCherry* insert used for biolistic transformation.

Following biolistic transformation, two PCRs, each confirming one end of the construct, were performed as an initial screening to assess successful homologous recombination with the *ACK1-mCherry* construct. Confirmation of the 5' end of the construct was performed using primers KIO33 and BLO45. The sequence of primer KIO33 is located upstream of the 5' end of the construct, and the sequence of antisense primer BLO45 is located within *mCherry*. Primers BLO46 and KIO12 were used to confirm placement of the 3' end of the construct. The sequence of primer BLO46 is

found within *NEO*^{R} and that of primer KIO12 is found downstream of the *ACK1-mCherry* construct. Each PCR contains a primer within the construct and the other primer outside of the construct. Therefore, amplification of the 5' and 3' ends using gDNA from the biolistics transformants and the above mentioned primers demonstrates that at least one copy of the *ACK1-mCherry* construct integrated successfully into the correct location within the genome.

Placement PCRs performed on one gDNA sample from each biolistics plate is demonstrated in Figures 43 and 44. The gel image of the 5' end confirmation PCRs (Figure 39) demonstrates well-amplified fragments located between the 3 Kb and 4 Kb bands of the DNA ladder corresponding to the expected fragment length of 3,181 bp in each of the transformant gDNA samples, with the exception of colony 63. In addition, this band is not present in the WT gDNA sample as expected since the antisense primer for this reaction consists of a sequence of *mCherry*. A variety of faint bands are seen in each of the samples, likely representing nonspecific binding of primers at similar sequences.

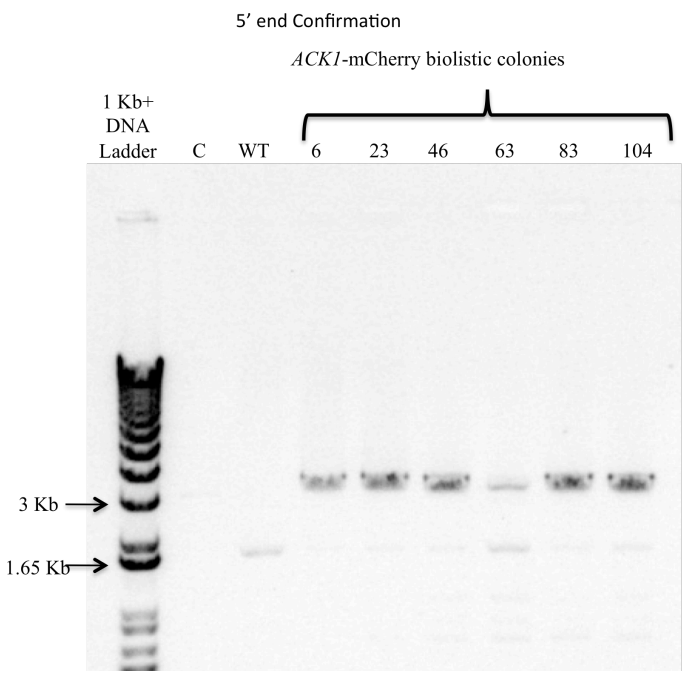

Figure 39: PCRs of *ACK1-mCherry* 5' End Placement Confirmation. PCR products of 5' untranslated region, *ACK1*, and *NEO*^{R} of the *ACK1-mCherry* construct using gDNA from biolistics colonies 6, 23, 46, 63, 83, and 104 for confirmation of 5' end integration within the genome.

The gel image of the 3' end confirmation PCRs (Figure 40) demonstrate well-amplified fragments located between the 2 Kb and 3 Kb ladder bands from colonies #6, #23, #46, #83, and #104. This corresponds to the expected length of 2,146 bp. No band is noted in the WT or colony #63 gDNA samples. As with the 5' end confirmation, this band is not demonstrated in the WT gDNA sample since the sense primer BLO46 consists of a *NEO*^{R} sequence that is not present within the WT genome. The absence of amplification of gDNA from colony #63 indicates that that particular transformant does not possess the entire *ACK1-mCherry* construct. No other bands are noted in the gel.

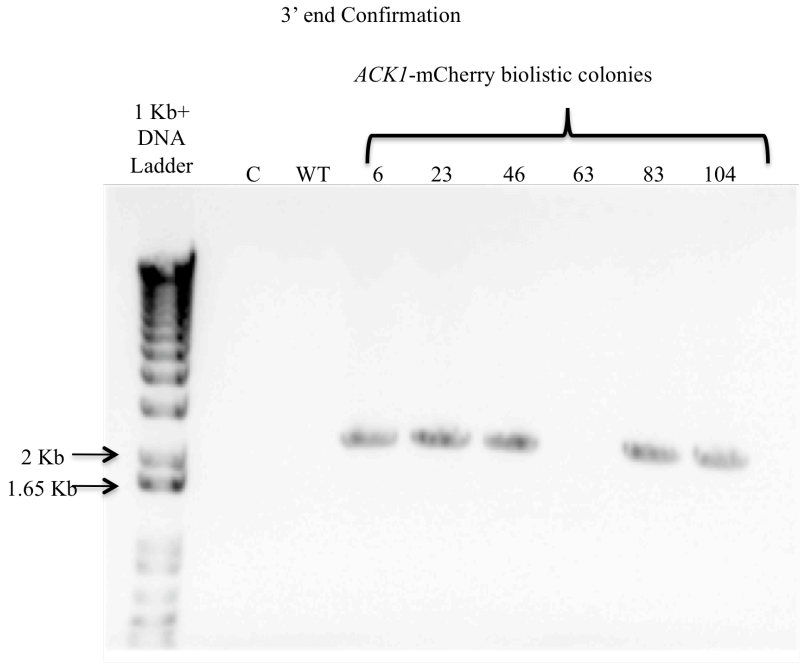

Figure 40: PCRs of *ACK1-mCherry* 3' End Placement Confirmation. PCR products of the *NEO*^{R} and 3' untranslated region of the *ACK1-mCherry* construct using gDNA from biolistics colonies 6, 23, 46, 63, 83, and 104 for confirmation of 3' end integration within the genome.

CONCLUSION

The goal of the research presented here was to confirm *ACK1* gene deletion strains that were created by Dr. Bose for use in this work and try to elucidate a phenotype that deviates from the wild type. A construct was produced for use as a complementation in the event that a unique phenotype was observed, a strain in which *ACK1* is tagged with the gene that codes for a red fluorescent protein, *mCherry*, was created in hopes of discovering where the protein is localized within the cell and to enable purification of the protein for enzyme assays.

cDNA analysis demonstrated the absence of mRNA coding for *ACK1*, and the Southern blot analysis confirmed a single successful homologous recombination, replacing *ACK1* with the NEO^R deletion cassette. Unfortunately, the phenotype characterization studies attempted in this work failed to demonstrate an alternate phenotype different from that exhibited by the wild-type strain (KN99). In the absence of a variant phenotype, the construct created in this work for extra-chromosomal *ACK1* expression for complementation studies was prepared but not utilized.

The lack of phenotypic difference between the WT and the *ack1Δ* strains is perplexing, however, due to the relatively new discovery of potential *ackA* homologs in eukaryotic microbes, little has been established as to their role within organisms of this domain.

It is quite possible that this homolog does not have analogous function in eukaryotes. *Entamoeba histolytica*, a eukaryotic organism in which a homolog for acetate kinase was found, did not demonstrate a homolog for *PTA* or *XFP*, the two

enzymes that produce the substrate utilized by AK (Ingram-Smith et al. 2006). It was hypothesized that, in light of those findings, AK in *E. histolytic* could play a novel role. (Ingram-Smith et al. 2006). While it was found that a homolog for *PTA* was not identified, two homologs for XFP were found, XFP1p and XFP2p. One method that could be used to determine if the homologs of XFP work together with AK in the acetate assimilation pathway is to construct separate mutant strains in which each *XFP*1 and *XFP2* is deleted as well as two strains that include double deletes of each of the *XFP*s and *ACK1*. These strains could be utilized for phenotype characterization studies along with the *ack1Δ* strains that were created for this study. Studies similar to this involving other proteins involved in the acetate assimilation pathway, such as *ACS*, could also be approached to gain a better understanding of how or if these enzymes work together.

Another potential approach to elucidating AK function would be to study the gene's expression pattern under various conditions. Clues as to protein function can often be obtained by discovering factors that influence gene expression [Alberts et al. 2002]. If acetate kinase plays a subtler role, detecting changes in expression could help narrow down the field of potential phenotype characterization experiments by honing in on stimuli that affect gene expression.

The *ACK1-mCherry* strain that was produced might reveal information about where in the cell this protein is utilized. PCR amplification of the 5' and 3' ends of *ACK1-mCherry* strains suggest correct placement of the construct within the genome. In-house fluorescence and confocal microscopy utilized for subcellular localization of the *mCherry*-tagged Ack1p was attempted, however, no visualization of the red fluorescent protein-tagged enzyme was observed. It is not known if the absence of red fluorescence

is due to the lack of AK production in the cells or due to hardware issues such as the necessity of a camera on the microscope or an update in the software for the confocal microscope. It was noted, however, that positive control strains for green fluorescence protein (GFP) also failed to demonstrate fluorescence. A western blot of cell lysate using antibodies against the *mCherry* protein could indicate the presence of the tagged protein. The *mCherry* tags can also be used to pull down the protein for use in enzyme assays. Protein studies of endogenous acetate kinase from *C. neoformans* could also help reveal its function. Learning more about the enzyme kinetics of the protein itself might provide clues as to its biological role.

The discovery of homologous proteins, previously thought limited to prokaryotes, in eukaryotic organisms has opened a new arena in which little is known. The interest in this particular enzyme stems from the fact that several of the eukaryotic microbes possessing this protein can be pathogenic as is the case with *C. neoformans*. The apparent absence of AK homologs in higher eukaryotic organisms motivates the desire to understand its role since proteins and metabolic pathways that are unique to pathogens can be potential targets by therapeutic agents. It is hopeful that continued research will help elucidate the function of acetate kinase in *C. neoformans*.

REFERENCES

1. Alberts B, Johnson A, Lewis J, Raff M, Roberts K, and Walter P. Molecular Biology of the Cell. 4th edition. New York: Garland Science; 2002. Studying Gene Expression and Function. Available from: http://www.ncbi.nlm.nih.gov/books/NBK26818/

2. Bose I, MCR. *C neoformans* Genomic DNA Preparation with Glass Beads [Internet]. St. Louis (MO); [Revised 2009, cited 3/23/13]. Available from: http://www.crypto.wustl.edu/Protocols%20PDFs/Genomic_DNA_-_small_(IB)3.pdf

3. Bragg, PD, Reeves, RE. 1962. Pathways of glucose dissimilation in Laredo strain of Entamoeba histolytica. Experimental Parasitology 12(5): 393–400.

4. Brock, DL. Infectious Fungi. In: Alcamo, IE, editor. Deadly Diseases and Epidemics. Chelsea House Publishers. 2006. pp 67-71.

5. Buss KA, Cooper DR, Ingram-Smith C, Ferry JG, Sanders DA, Hasson MS. 2001. Urkinase: Structure of Acetate Kinase, a Member of the ASKHA Superfamily of Phosphotransferases. Journal of Bacteriology 183(2): 680-686.

6. Chen J, Varma A, Diaz MR, Litvintseva AP, Wollenberg KK, Kwon-Chung KJ. 2008. *Cryptococcus neoformans* Strains and Infection in Apparently Immunocompetent Patients, China. Emerging Infectious Diseases 14(5): 755-762.

7. Chen YL, Lehman VN, Lewit Y, Averette AF, Heitman J. 2013. Calcineurin Governs Thermotolerance and Virulence of *Cryptococcus gattii*. G3: Genes, Genomes, Genetics 3: 527-539.

8. Casadevall, A, Perfect, JR. (1998) *Cryptococcus neoformans*. American Society for Microbiology Press. Washington, DC.

9. Datta K, Bartlett KH, Baer R, Byrnes E, Galanis E, Heitman J, Hoang L, Leslie MJ, MacDougall L, Magill SS, Morshed MG, Marr KA. (2009). Spread of *Cryptococcus gattii* into Pacific Northwest Region of the United States. Emerging Infectious Diseases. 15: 1185-1191. Issue 8. http://wwwnc.cdc.gov/eid/article/15/8/08-1384.htm

10. Fox DS, Djordjevic JT, Sorrell TC. 2011. Signaling Cascades and Enzymes as Cryptococcus Virulence Factors. In: Heitman J, Kozel TR, Kwong-Chung KJ, Perfect JR, Casadevall, A, editors. *Cryptococcus*: From Human Pathogen to Model Yeast. Washington, D.C. ASM Press. 217-234.

11. Garcia-Hermoso D, Janbon G, Dromer F. 1999. Epidemiological Evidence for Dormant *Cryptococcus neoformans* Infection. Journal of Clinical Microbiology. 37(10): 3204-3209.

12. Govender, NP, Patel, J, van Wyk, M, Chiller, TM, Lockhart, SR. 2011. Trends in Antifungal Drug Susceptibility of *Cryptococcus neoformans* Isolates Obtained Through Population-Based Surveillance In South Africa in 2002-2003 and 2007-2008. Antimicrobial Agents Chemotherapy. 55(6): 2606-26011.

13. Griffith. Doering Laboratory Specialty Media [Internet]. St. Louis(MO); [5/11/12, cited 4/13/11] . Available from: http://www.crypto.wustl.edu/Protocols%20PDFs/Specialty_plates_(CG).pdf

14. Griffith. Doering Laboratory - Basic Media and Plates [Internet]. St.Louis(MO); [5/11/12, cited 4/13/11] . Available from: http://www.crypto.wustl.edu/Protocols%20PDFs/Basic%20media%20(CG).pdf

15. Hull CM, Heitman J. Genetics of *Cryptococcus neoformans*. Annual Review of Genetics 36: 557-615.

16. Ingavale SS, Chang YC, Lee H, McClelland CM, Leong ML, Kwon-Chung KJ. (2008) Importance of Mitochondria in Survival of *Cryptococcus neoformans* Under Low Oxygen Conditions and Tolerance to Cobalt Chloride. PLoS Pathog 4(9): e1000155. doi:10.1371/journal.ppat.1000155

17. Ingram-Smith, C, Martin, SR, Smith, KS. (2006). Acetate Kinase: Not Just a Bacterial Enzyme. TRENDS in Microbiology. 14*:* 249-253.

18. Loftus B, Fung E, Roncaglia P, Rowley D, Amedeo P, Bruno D, Vamathevan J, Miranda M, Anderson IJ, Fraser JA, Allen JE, Bosdet IE, Brent MR, Chiu R, Doering TL, Donlin MJ, D'Souza CA, Fox DS, Grinberg V, Fu J, Fukushima M, Haas BJ, Huang JC, Janbon G, Jones SJM, Koo HL, Krzywinski MI, Kwon-Chung JK, Lengeler KB, Maiti R, Marra MA, Marra RE, Mathewson CA, Mitchell TG, Pertea M, Riggs FR, Salzberg SL, Schein JE, Shvartsbeyn A, Shin H, Shumway M, Specht CA, Suh BB, Tenney A, Utterback TR, Wickes BL, Wortman JR, Wye NH, Kronstad JW, Lodge JK, Heitman J, Davis RW, Fraser CM, Hyman RW. 2005. The Genome of the Basidiomycetous Yeast and Human Pathogen *Cryptococcus neoformans*. Science. 307(5713): 1321-1324.

19. McQuiston T, Del Poeta M. 2011. The Interaction of *Cryptococcus neoformans* with Host Macrophages and Neutrophils. In: Heitman J, Kozel TR, Kwong-Chung KJ, Perfect JR, Casadevall, A, editors. *Cryptococcus*: From Human Pathogen to Model Yeast. Washington, D.C. ASM Press. 373-385.

20. Meile L, Rohr, LM, Geissmann, TA, Herensperger M, Teuber M. 2001. Characterization of the D-Xylulose 5-Phosphate/D-Fructose 6-Phosphate Phosphoketolase Gene (*xfp*) from *Bifidobacterium lactis. Journal of Bacteriology 183(9): 2929-2936.*

21. Mody CH, Toews GB, Lipscomb MF. (1988) Cyclosporin A inhibits the growth of *Cryptococcus neoformans* in a Murine Model. Infection and Immunology 56(1): 7 -12.

22. Neuville S, Dromer F, Morin O, Dupont B, Ronin O, Lortholary O, and the French Cryptococcosis Study Group. 2003. Primary Cutaneous Cryptococcosis: A Distinct Clinical Entity. Clinical Infectious Diseases 36: 337-347.

23. Pappas PG. 2011. Antifungal Trials: Progress, Approaches, New Targets, and Perspectives in *Cryptococcus*. In: Heitman J, Kozel TR, Kwong-Chung KJ, Perfect JR, Casadevall, A, editors. *Cryptococcus*: From Human Pathogen to Model Yeast. Washington, D.C. ASM Press. 527-536.

24. Park, BJ, Wannemuehler, KA, Marston, BJ, Govender, N, Pappas, PG, Chiller, TM. (2009). Estimation of the Current Global Burden of Cryptococcal Meningitis Among Persons Living With HIV/AIDS. AIDS. 23(4): 525-530.

25. Saag MS, Graybill RJ, Larsen RA, Pappas PG, Perfect JR, Powderly WG, Sobel JD, Dismukes WE, and Mycoses Study Group Cryptococcal Subproject. 2000. Practice Guidelines for the Management of Cryptococcal Disease. Clinical Infectious Diseases 30(4): 710-718.

26. Thaker TM, Tanabe M, Fowler ML, Preininger AM, Ingram-Smith C, Smith KS, Iverson TM. 2013. Crystal Structures of Acetate Kinases from the Eukaryotic Pathogen Entamoeba histolytica and *Cryptococcus neoformans*. The Journal of Structural Biology 181: 185-189.

27. Wang Y, Casadevall A. 1994. Susceptibility of Melanized and Nonmelanized *Cryptococcus neoformans* to Nitrogen- and Oxygen-Derived oxidants. Infection and Immunity 62(7): 3004.

28. Wickes BL, Mayorga ME, Edman U, Edman JC. 1996. Dimorphism and Haploid Fruiting in *Cryptococcus neoformans*: Association with the a-Mating Type. Proceedings from the National Academy of Science: Microbiology 93: 7327-7331.

29. Wolfe, AJ. 2005. The Acetate Switch. Microbiology and Molecular Biology Reviews. 69(1): 12-50.

30. Zaragoza O, Rodrigues ML, De Jesus M, Frases S, Dadachova E, Casadevall A. 2009. The Capsule of the Fungal Pathogen *Cryptococcus neoformans*. Advances in Applied Microbiology 68: 133–216

31. Zaragosa O, Casadevall A. 2004. Experimental Modulation of Capsule Size in *Cryptococcus neoformans*. Biology Procedures Online [Internet]. [cited 3/22/12] 6(1):10-15. Available from: http://www.ncbi.nlm.nih.gov/pmc/articles/PMC389900/

APPENDIX A

List of primers

Primer Number	Primer Sequence (5' to 3')	Gene
BLO01	CTTGGTCATTGACAATGGCTC	*ACT1*
BLO02	GTCTCGTGGATACCAGCAGC	*ACT1*
BLO11	GACTAGTGCCATACAGACGAATGACTG	*ACK1*
BLO12	GACTAGTCCGTCGATATATGAGAAGCC	*ACK1*
BLO45	CACCCTTGGTCACCTTCAGC	*ACK1*
BLO46	GGATCTCGTCGTGACCCATG	*NEO*^{R}
KIO12	CATGCTCTGATTGGCTTCTCAC	*ACK1*
KIO21	CGTAAGTAGAGTCGAAACTCG	*ACK1*
KIO22	GCTTTAGAGACGGTGAAGTC	*ACK1*
KIO23	CTGCATCCATCTGCCTTGTC	*NEO*^{R}
KIO24	CATGATATTCGGCAAGCAGG	*NEO*^{R}
KIO25	CTCGCTGTGACCAATATCAGC	*ACK1*
KIO26	GCTAGCTTCTTCAGCACATCC	*ACK*
KIO27	CGGGATCCAGAGTGTTGTGCACGTCAC	*ACK1*
KIO28	GACTAGTAAACCCAAATTCCTCCTTG	*ACK1*
KIO29	GACTAGTCATGGTGAGCAAGGGCGAG	*mCherry*
KIO30	GGAATTCCATATGTGGTTTATCTGTATTAACACGG	*NEO*^{R}
KIO31	GGAATTCCATATGGCGAACTTAGTGGGTCTTGAC	*ACK1*
KIO32	CGGGGTACCATCAATAAAAGCTTTCTTCACTCC	*ACK1*
KIO33	GCAAACACCAAGAATGTCTCG	*ACK1*